LA-6472-PR
Progress Report

C.3

CIC-14 REPORT COLLECTION
REPRODUCTION
COPY

Special Distribution
Issued: August 1976

Applied Nuclear Data Research and Development

January 1—March 31, 1976

Compiled by

C. I. Baxman
G. M. Hale
P. G. Young

LOS ALAMOS NATL. LAB. LIBS.
3 9338 00375 1905

los alamos
scientific laboratory
of the University of California
LOS ALAMOS, NEW MEXICO 87545

An Affirmative Action/Equal Opportunity Employer

UNITED STATES
ENERGY RESEARCH AND DEVELOPMENT ADMINISTRATION
CONTRACT W-7405-ENG. 36

The four most recent reports in this series, unclassified, are LA-6018-PR, LA-6123-PR, LA-6164-PR, and LA-6266-PR.

This work was performed under the auspices of the Defense Nuclear Agency, the Nuclear Regulatory Commission, the National Aeronautics and Space Administration, and the US Energy Research and Development Administration's Divisions of Military Application, Reactor Development and Demonstration, Physical Research, and Magnetic Fusion Energy.

This report was prepared as an account of work sponsored by the United States Government. Neither the United States nor the United States Energy Research and Development Administration, nor any of their employees, nor any of their contractors, subcontractors, or their employees, makes any warranty, express or implied, or assumes any legal liability or responsibility for the accuracy, completeness, or usefulness of any information, apparatus, product, or process disclosed, or represents that its use would not infringe privately owned rights.

CONTENTS

LOS ALAMOS NATIONAL LABORATORY
3 9338 00375 1905

APPLIED NUCLEAR DATA RESEARCH AND DEVELOPMENT
QUARTERLY PROGRESS REPORT
January 1 - March 31, 1976

Compiled by

C. I. Baxman, G. M. Hale, and P. G. Young

ABSTRACT

This progress report describes the activities of the Los Alamos Nuclear Data Group for the period January 1 through March 31, 1976. The topical content is summarized in the contents.

I. THEORY AND EVALUATION OF NUCLEAR CROSS SECTIONS

A. Evaluation of Light Element Standard Cross Sections

Because the $^{6}Li(n,\alpha)$ cross sections are large and relatively structureless at energies below 100 keV, they are widely used as "standards" relative to which other neutron cross sections are measured. To extend the useful energy range of these standards and to improve their accuracy at lower energies, we are basing our evaluations on comprehensive R-matrix analyses of the ^{7}Li and ^{11}B systems which extend up into the region of known resonances.

1. $^{6}Li(n,\alpha)$ (G. Hale and D. Dodder [T-9])

A new evaluation of the neutron cross sections for ^{6}Li at low energies has just been completed, based on an extension of the comprehensive R-matrix analysis of the ^{7}Li system described at the Conference on Nuclear Cross Sections and Technology.[1] The $n + {}^{6}Li^{*}$ (2.185-MeV) channel has been added in the present analysis since the input data now extend to the energies above its threshold. These data include final values of the precise $^{4}He(t,t)$ differential cross sections[2] and new measurements of the $^{4}He(t,t)^{4}He$ analyzing power[3] done at the Los Alamos Scientific Laboratory (LASL). Examples of the fit to these data are shown in Fig. 1.

Recent measurements of the neutron total cross section[4] and of the $^{6}Li(n,\alpha)$ integrated cross section[5] were also included in the analysis. Figure 2 shows that the calculated $^{6}Li(n,\alpha)$ cross section is quite consistent with the new

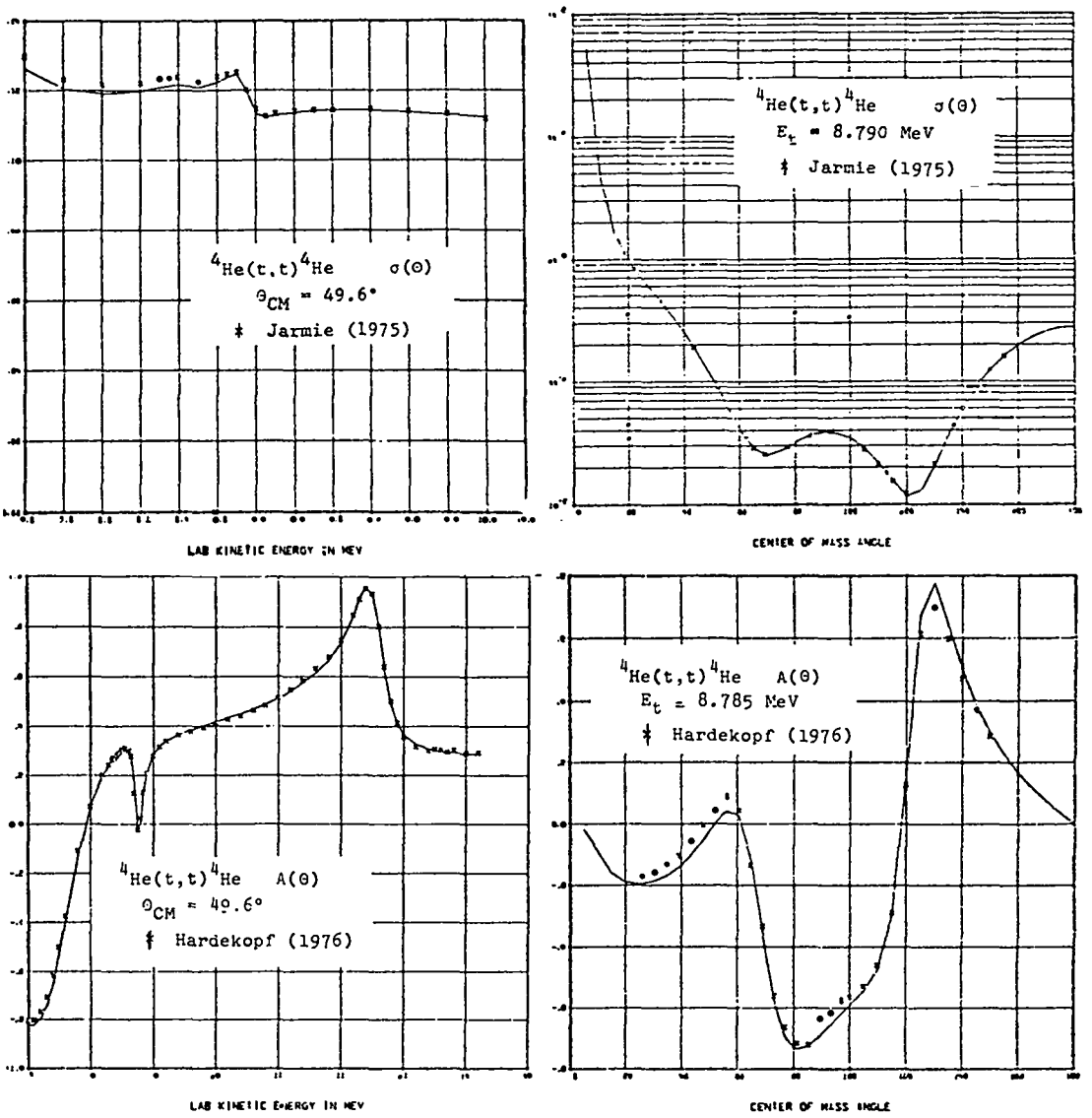

Fig. 1. R-matrix fit (solid line) to measurements of the ^{4}He(t,t)^{4}He differential cross section[2] (top) and triton analyzing power[3] (bottom).

measurements below 600 keV, while small but systematic differences between the calculated and measured total cross section are apparent. The calculated values of the ^{6}Li(n,α) cross section have been proposed for use as an ENDF/B-V standard at energies below 150 keV; they are estimated to be determined to within ± 3% even at energies over the resonance.

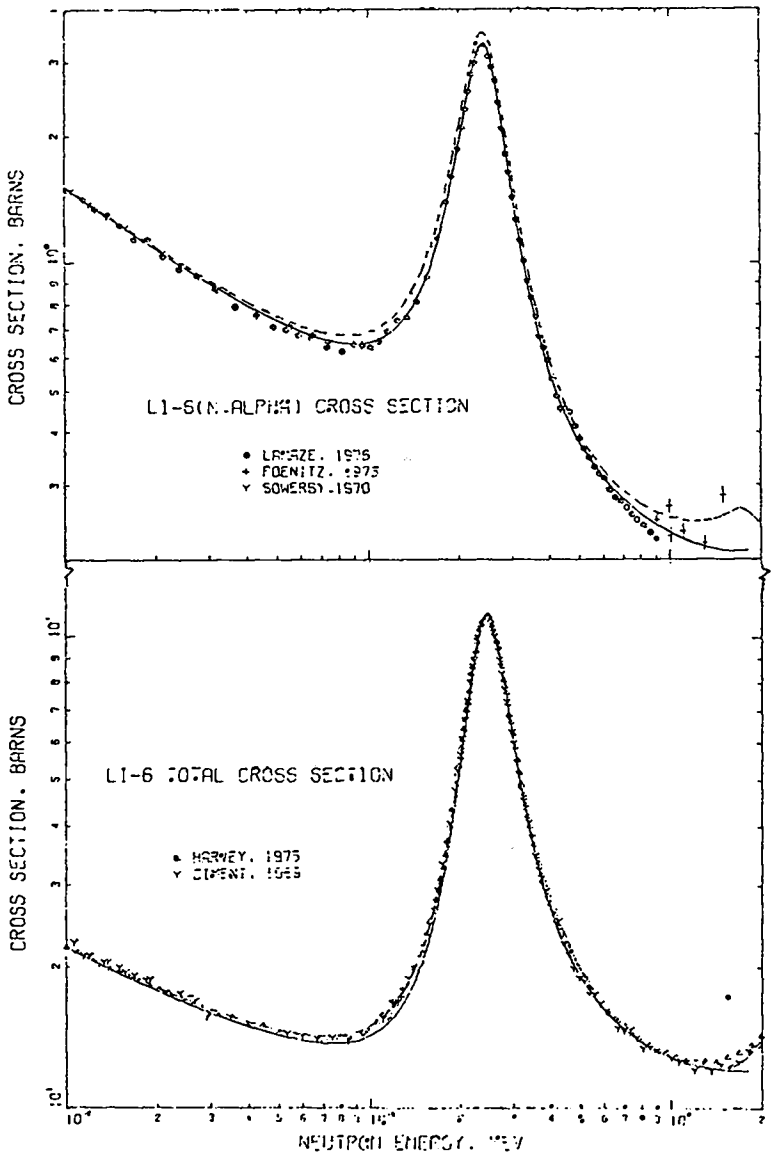

Fig. 2. Comparison of calculated and measured values of the $^{6}Li(n,\alpha)$ cross sections (top) and n-^{6}Li total cross section (bottom) between 0.01 and 1 MeV. The solid curve is the present analysis; the dashed curve is ENDF/B-IV.

2. $^{10}B(n,\alpha)$ (G. M. Hale and E. D. Arthur)

A new evaluation of the neutron cross sections for ^{10}B at low energies has also been completed recently. The evaluation is based on a multichannel, multilevel R-matrix analysis of reactions in the ^{11}B system similar to that which was used to provide the boron cross sections for ENDF/B-IV. New data that were considered in the present analysis include relative measurements of

the $^{10}B(n,\alpha\gamma)$ integrated cross section[6] and absolute measurements of the $^{10}B(n,\alpha\gamma)$ angular distribution.[7]

The resulting fit to the $^{10}B(n,\alpha)$ integrated cross sections is seen in Fig. 3 to be almost identical to the Version IV calculations at energies below 200 keV, while it decreases more rapidly than before at energies up to 1 MeV. The calculated values of the $^{10}B(n,\alpha)$ cross section have been proposed for use as an ENDF/B-V standard at energies below 150 keV.

B. Evaluation of Neutron-Induced Reactions on ^{6}Li and ^{12}C

1. n + ^{6}Li (L. Stewart and P. G. Young)

Because much of the ^{6}Li evaluated data in the ENDF/B-IV general purpose file is based on a rather old United Kingdom set,[8] we have re-evaluated the ^{6}Li data incorporating more recent experimental results. As described earlier,[9] modifications were made to the total, elastic, (n,n'd), (n,p), and (n,t) cross sections, to the elastic angular distributions, and to the energy and angular distributions of secondary neutrons from (n,n'd) and (n,2n) reactions.

The most significant revision was in the representation of secondary neutrons from the $^{6}Li(n,n'd)^{4}He$ reaction, which are given as evaporation spectra in ENDF/B-IV. In order to include energy-angle correlations in the data without introducing new requirements on the ENDF/B processing codes, we utilized "pseudo levels" and phase-space arguments to represent the neutron continuum from the (n,n'd) reaction, assuming isotropic center-of-mass angular distributions. In Fig. 4, experimentally measured[10] neutron spectra at 39 and 150° for 7.5-MeV incident neutrons are compared to nonelastic neutron spectra from the new analysis and from the older ENDF/B-IV temperature representation. Similarly, Fig. 5 shows the Version IV, pseudo-level comparison for 14-MeV incident neutrons and θ = 0 and 180°. In each case, the ENDF/B-IV data do not describe the inelastic group to the 2.2-MeV state of ^{6}Li at all, and predict too hard a spectrum at back angles. Indeed, nonelastic neutrons in the back-angle spectra have energies higher than the elastic peaks. Similar effects appear in comparisons at other energies and angles.

2. n + ^{12}C (P. G. Young)

To provide interim data for local use prior to the release of ENDF/B-V, the pseudo-level representation was also used to improve secondary neutron spectra from the $^{12}C(n,n')3\alpha$ reaction. In this case, the ENDF/B-IV integrated cross

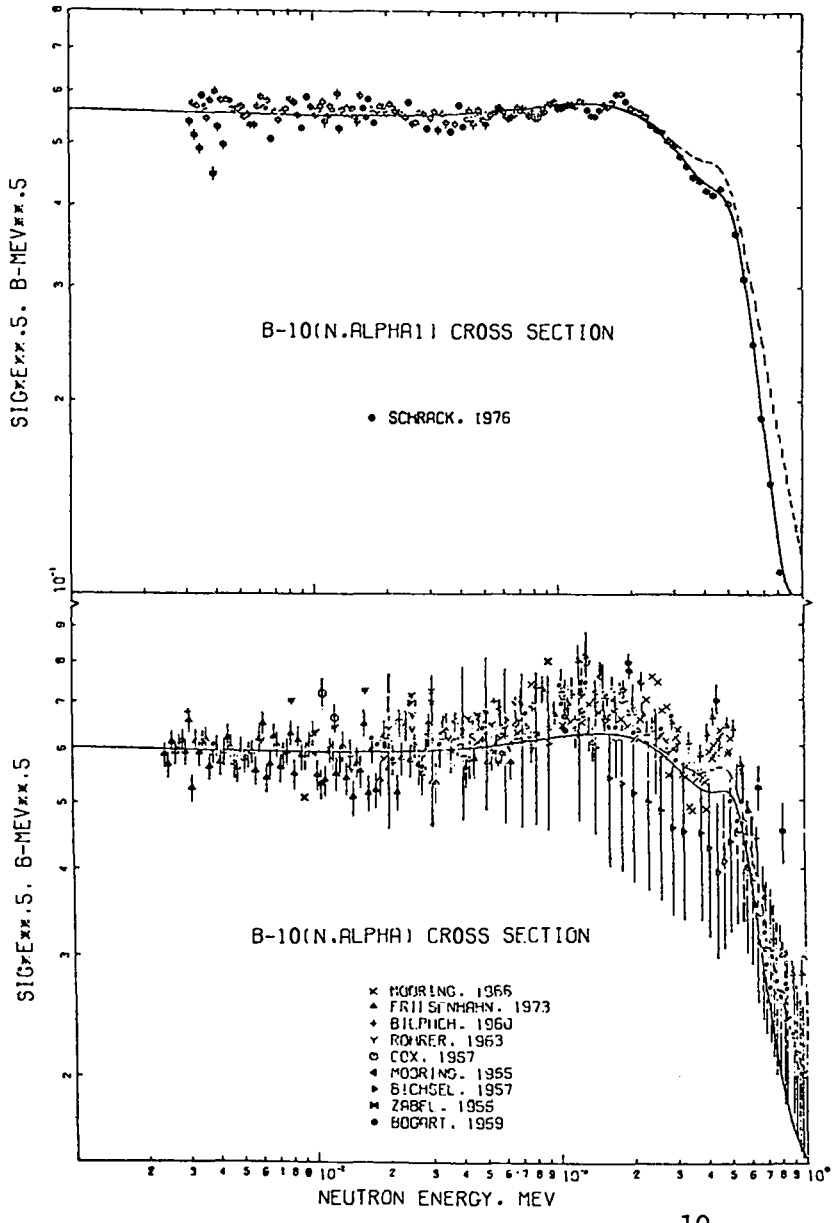

Fig. 3. Calculated and measured values of the $^{10}B(n,\alpha\gamma)$ (top) and $^{10}B(n,\alpha)$ (bottom) cross sections between 1 keV and 1 MeV. The solid curve is the present analysis; the dashed curve is ENDF/B-IV.

section for the reaction was divided among the available pseudo levels assuming pure 4-body phase-space distributions of final states and isotropic center-of-mass angular distributions. The level excitation cross section and angular distribution for the real ^{12}C level at E_X = 4.44 MeV were kept the same as given in Version IV.

The nonelastic energy distributions from the pseudo-level representations are compared in Fig. 6 to ENDF/B-IV data for 14-MeV incident neutrons and θ = 0

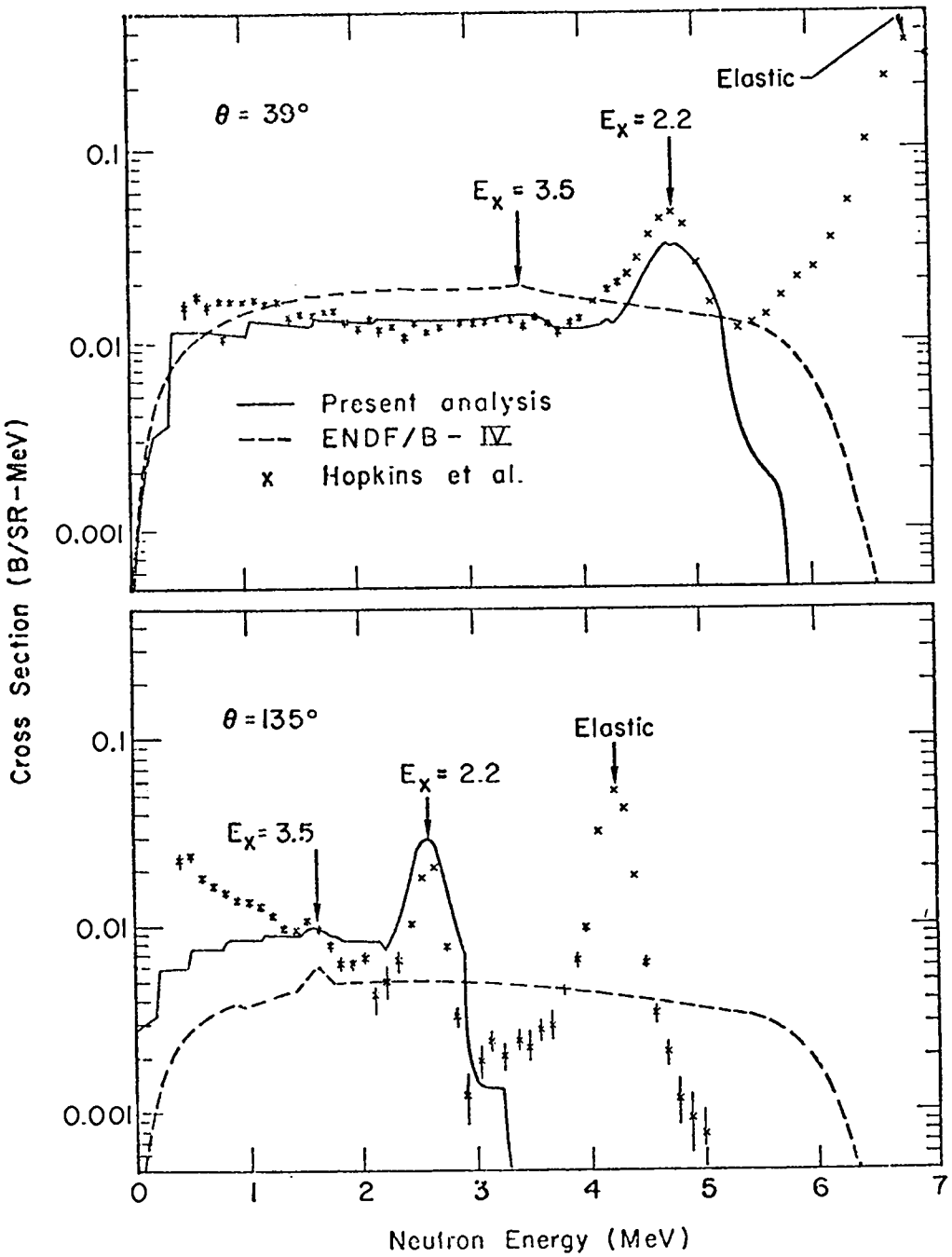

Fig. 4. Neutron emission spectra from the interaction of 7.5-MeV neutrons on ^{6}Li. The evaluated curves only include nonelastic neutrons.

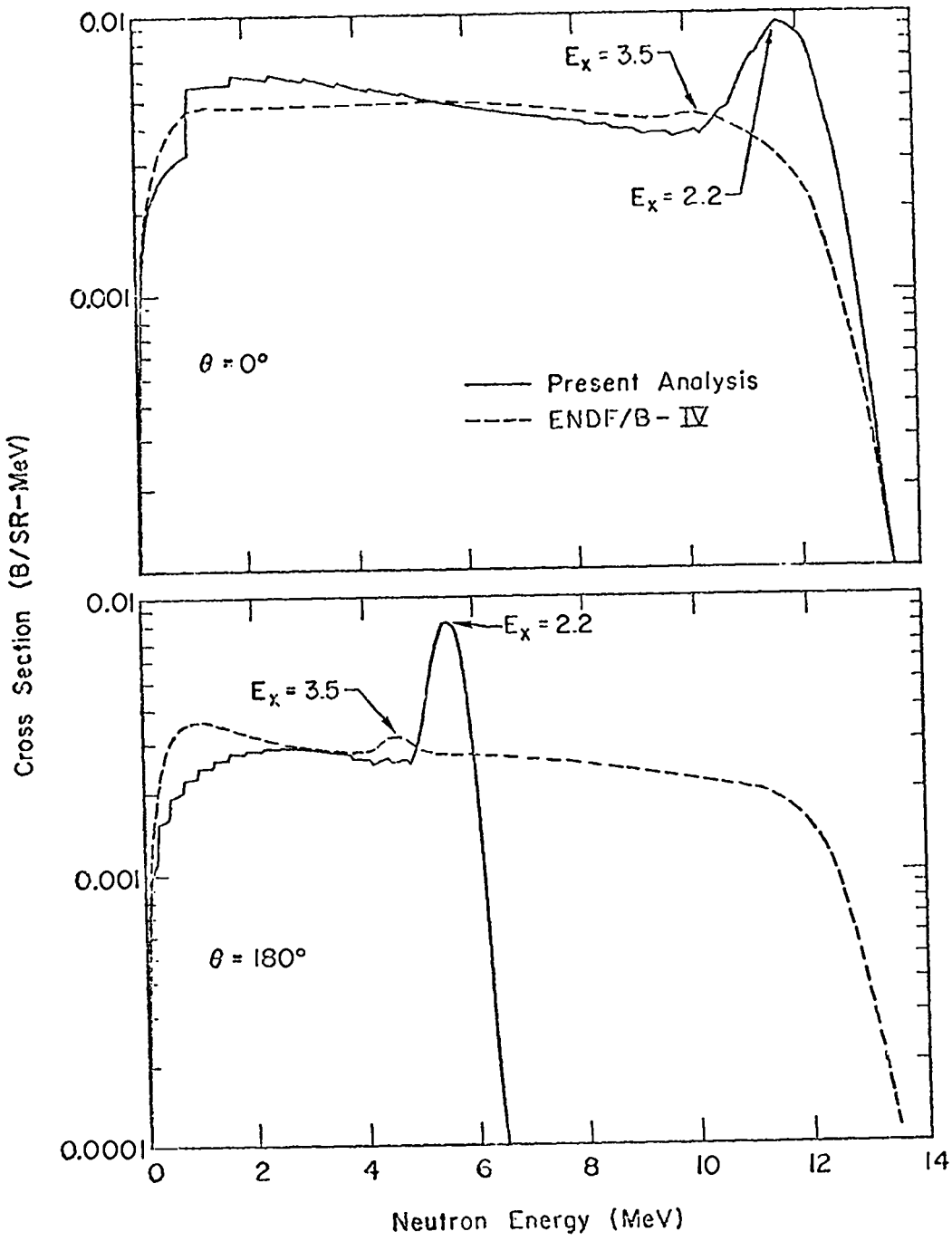

Fig. 5. Nonelastic neutron emission spectra from the interaction of 14-MeV neutrons ^{6}Li.

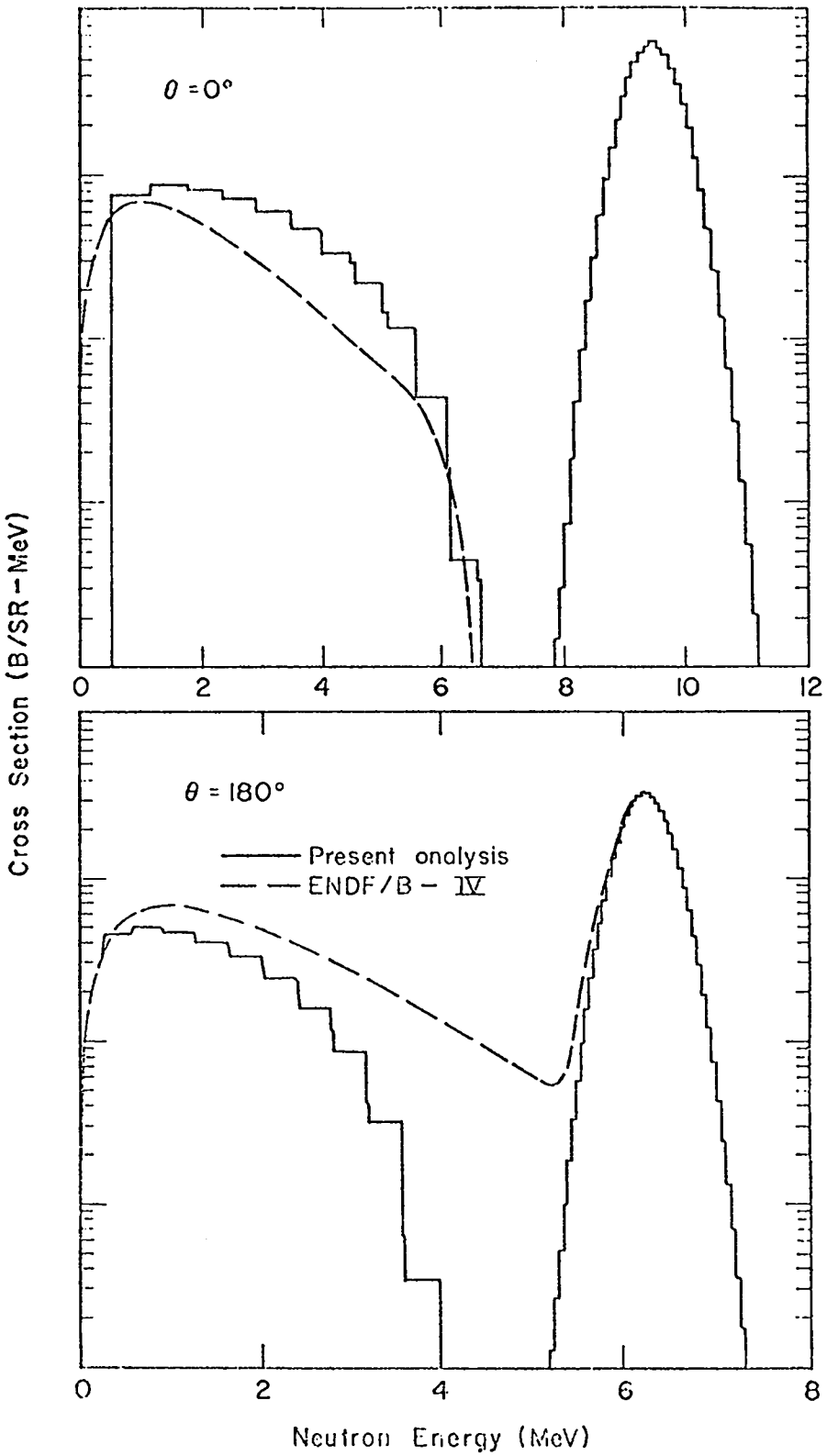

Fig. 6. Nonelastic neutron emission spectra from the interaction of 14-MeV neutrons on ^{12}C.

and 180°. The peak at higher energy in the spectra corresponds to the inelastic neutron group to the 4.44 MeV level in ^{12}C, broadened with a 10% FWHM gaussian resolution function. Again, the ENDF/B-IV temperature spectra are harder at back angles than the energy-angle correlated data.

Very few experimental data are available for determining the secondary neutron spectra, so the uncertainty in these results is large. However, emulsion data from a 1955 measurement[11] for incident neutron energies between 12 and 20 MeV are well represented by a 4-body phase-space distribution. More recent 14-MeV data indicate that (n,n') reactions through the broad, unbound levels of ^{12}C are important,[12] but these results were not included in the present limited analysis.

C. Ground-State Properties of Nuclei (D. G. Foster, Jr.)

A new variation of the nuclear mass-excess subroutine package described last quarter has been completed. In the old version, the standard deviations for the mass excesses were packed into the lowest 18 bits of the CDC 60-bit words, in order to permit weighted fitting for extrapolation outside the 2055-entry table. In the new version, these standard deviations are replaced by ground-state spins and parities of the same tabulated nuclei, as found in the 1971 Nuclear Wallet Cards prepared by Ajzenberg-Selove and Busch.[13] All of the even-Z, even-N nuclei were assigned 0^+ entries, whether actually measured or not. The immediate purpose of this version is to supply input information to the GNASH code as part of a program to automate as much of the setup for GNASH as possible. It was noted in passing that there are now five known 0^- ground states, all of them for odd-odd nuclei.

D. Calculation of (n,2n) and (n,3n) Cross Sections and Spectra (E. D. Arthur, P. G. Young, and L. R. Veeser [P-3])

The capability to calculate the spectra of first and second neutrons from (n,2n) reactions, and the spectra of first, second, and third neutrons from (n,3n) reactions has been developed. To calculate these spectra, populations computed by the preequilibrium-statistical nuclear model code GNASH were written onto disk, and then used by a second code to calculate the desired spectra. In this way, spectra effects resulting from gamma-ray or charged-particle competition can be included exactly.

The results of these spectrum calculations have been used by Veeser et al.[14] to make efficiency corrections for (n,xn) cross sections measured at high energies using large liquid scintillator tanks. The ability to calculate these spectra also meets certain requirements of the ENDF/B evaluated data files. Thus far, calculations have been carried out for (n,xn) reactions on ^{89}Y, ^{169}Tm, ^{171}Lu, and ^{197}Au. Figures 7 and 8 show the calculated first, second, and third neutron spectra for 24-MeV (n,xn) reactions on ^{197}Au. Figure 9 shows the overall agreement of the GNASH calculated curves with Au(n,xn) cross-section measurements by Bayhurst et al.[15] and Veeser et al.[14]

E. Calculation of Charged-Particle Spectra Induced by 14-15 MeV Neutrons (E. D Arthur and P. G. Young)

Calculation of proton-and alpha-particle production spectra from 14-15 MeV neutron bombardment have been made with the statistical-preequilibrium model code GNASH. Materials under study are those of CTR interest and include ^{27}Al, ^{46}Ti, ^{48}Ti, ^{51}V, and ^{93}Nb. For these calculations, the inclusion of preequilibrium effects is important to correctly reproduce the shape of the experimentally measured spectra. Here the closed preequilibrium form of Milazzo-Colli[16] has been used. Figure 10 shows the calculated proton-production spectrum for 15-MeV neutrons on ^{27}Al compared with preliminary results measured by Haight et al.[17] The calculated results were obtained with global input parameters with no attempt to adjust quantities to improve agreement with experiment.

F. Calculation of Activation Cross Sections for Pb Isotopes (E. D. Arthur, D. G. Foster, Jr., and P. G. Young)

In response to a request by TD-6, activation cross sections induced by neutrons on ^{204}Pb, ^{206}Pb, ^{207}Pb, and ^{208}Pb were determined and supplied in ENDF/B format. The reactions of interest are listed in Table I. For the most part, the preequilibrium-statistical model code GNASH was used to calculate the desired cross sections. However, for ^{204}Pb and $^{208}Pb(n,\gamma)$ reactions below 1 MeV, values were obtained from recent experimental measurements.[18] For the calculations,neutron transmission coefficients were obtained from global optical-model parameters of Wilmore and Hodgson,[19] the Brink-Axel giant dipole resonance form[20] was used for gamma-ray widths, and a closed preequilibrium form[16] provided corrections for semi-direct effects. In cases where comparison could be made with experimental data, there was reasonable agreement as shown by the examples in Figs. 11 and 12.

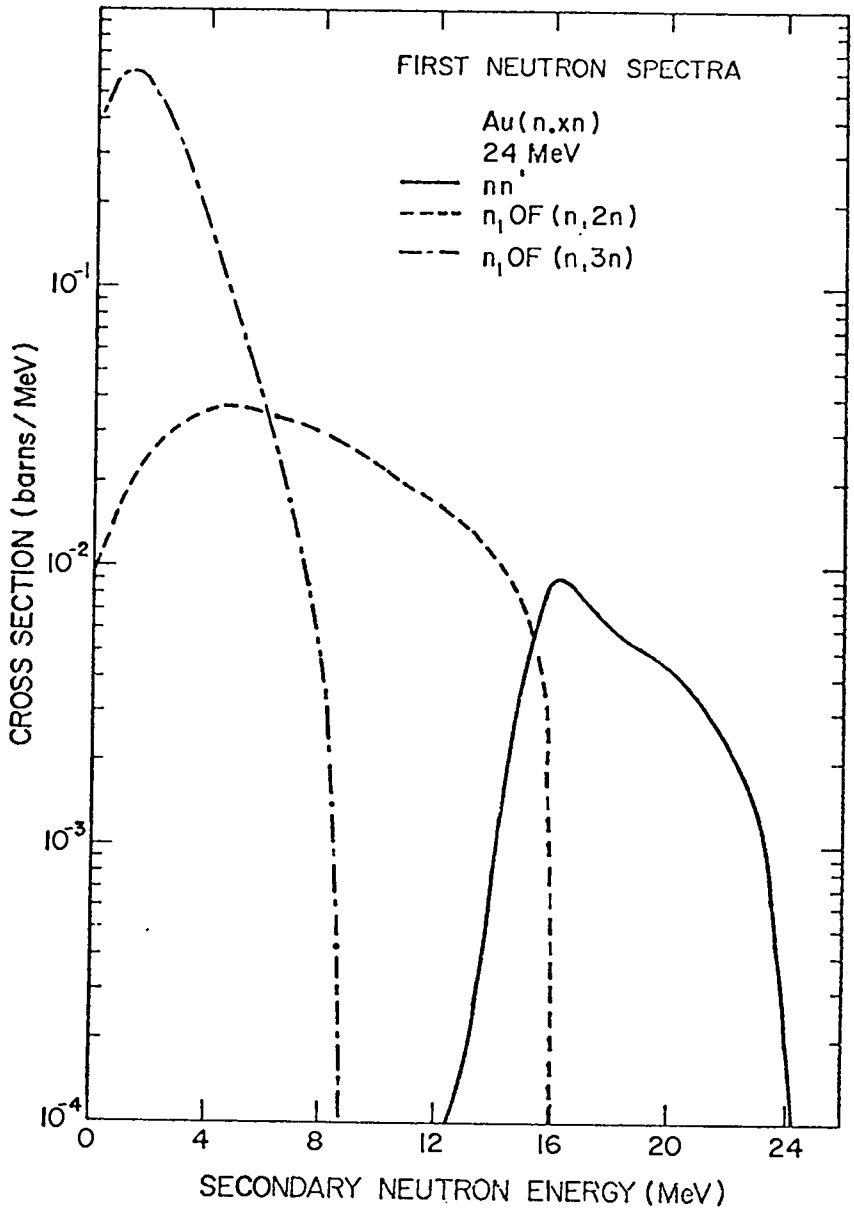

Fig. 7. Calculated first neutron spectra for 24-MeV Au(n,xn) reactions.

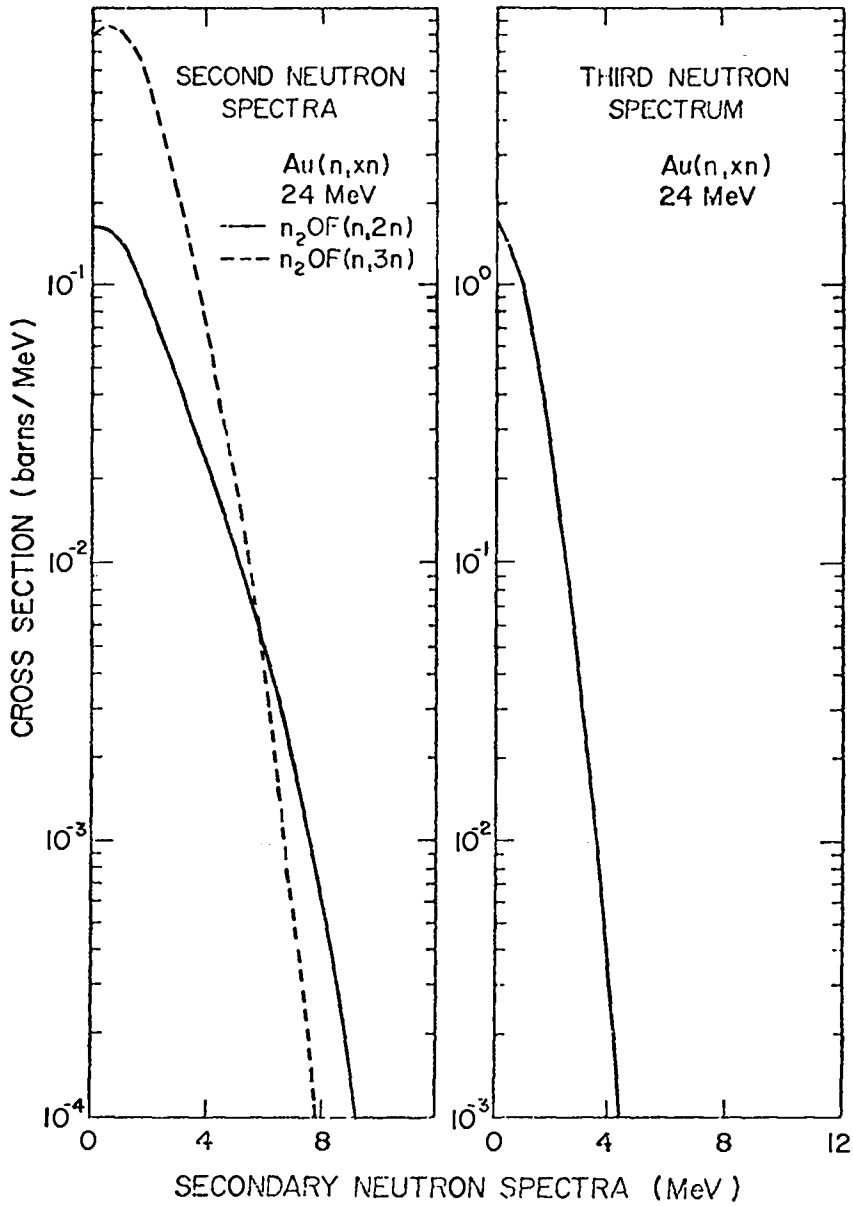

Fig. 8. Calculated second and third neutron spectra for 24-MeV neutron-induced Au(n,xn) reactions.

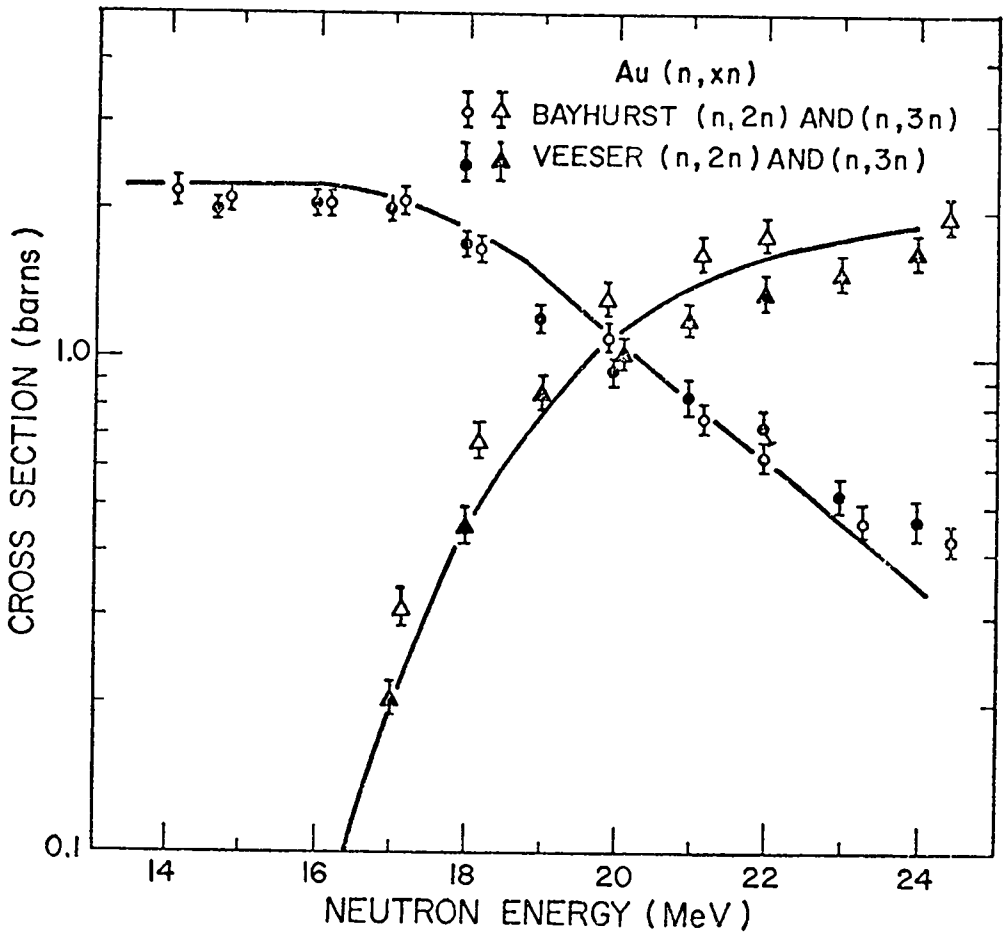

Fig. 9. Calculated and experimental values for Au(n,xn) reactions.

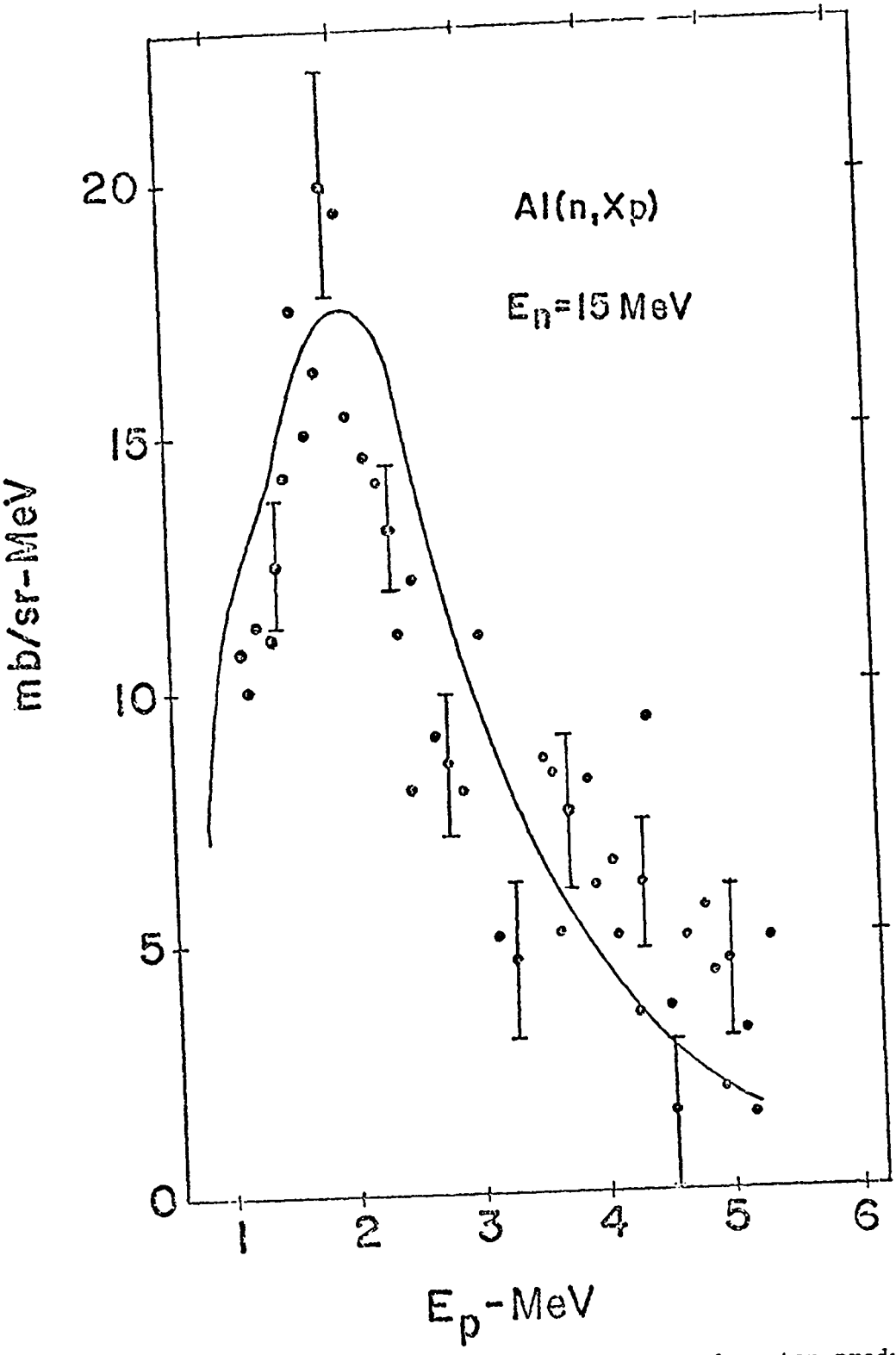

Fig. 10. A comparison of calculated and measured proton-production spectra induced by 15-MeV neutrons on ^{77}Al.

TABLE I

ACTIVATION REACTIONS IN Pb ISOTOPES

MAT	MT	REACTION	E_x (MeV)	T 1/2	Q (MeV)	THRESHOLD (MeV)
301	16	$^{204}Pb(n,2n)^{203}Pb$	0.0	52.1 h	- 8.401	8.443
301	17	$^{204}Pb(n,3n)^{202M}Pb$	2.17	3.62 h	-17.36	17.446
301	26	$^{204}Pb(n,2n)^{203M}Pb$	0.85	6.1 s	- 9.253	9.299
301	60	$^{204}Pb(n,n')^{204M}Pb$	2.19	66.9 m	- 2.186	2.197
301	102	$^{204}Pb(n,\gamma)^{205}Pb$	0.0	3.0×10^{7} y	6.735	--
301	700	$^{204}Pb(n,p)^{204}Tl$	0.0	3.81 y	.0195	-----
302	17	$^{206}Pb(n,3n)^{204M}Pb$	2.19	66.9 m	-17.08	17.164
302	26	$^{206}Pb(n,2n)^{205M}Pb$	1.01	4.0 ms	- 9.095	9.140
302	60	$^{206}Pb(n,n')^{206M}Pb$	2.20	130.0 μs	- 2.200	2.211
302	700	$^{206}Pb(n,p)^{206}Tl$	0.0	4.19 m	- 0.751	0.755
302	780	$^{206}Pb(n,\alpha)^{203}Hg$	0.0	46.9 d	7.136	--
303	17	$^{207}Pb(n,3n)^{205M}Pb$	1.01	4.0 ms	-15.84	15.92
303	26	$^{207}Pb(n,2n)^{206M}Pb$	2.20	130.0 μs	- 8.941	8.985
303	28	$^{207}Pb(n,np)^{206}Tl$	0.0	4.19 m	- 7.49	7.527
303	53	$^{207}Pb(n,n')^{207M}Pb$	1.63	0.80 s	- 1.633	1.641
303	700	$^{207}Pb(n,p)^{207}Tl$	0.0	4.79 m	- 0.650	0.653
303	702	$^{207}Pb(n,p)^{207M}Tl$	1.34	1.3 s	- 1.991	2.001
304	17	$^{208}Pb(n,3n)^{206M}Pb$	2.20	130.0 μs	-16.31	16.39
304	26	$^{208}Pb(n,2n)^{207M}Pb$	1.63	0.8 s	- 9.00	9.045
304	102	$^{208}Pb(n,\gamma)^{209}Pb$	0.0	3.3 h	3.938	--
304	700	$^{208}Pb(n,p)^{208}Tl$	0.0	3.1 m	- 4.211	4.230
304	780	$^{208}Pb(n,\alpha)^{205}Hg$	0.0	5.5 m	6.186	--

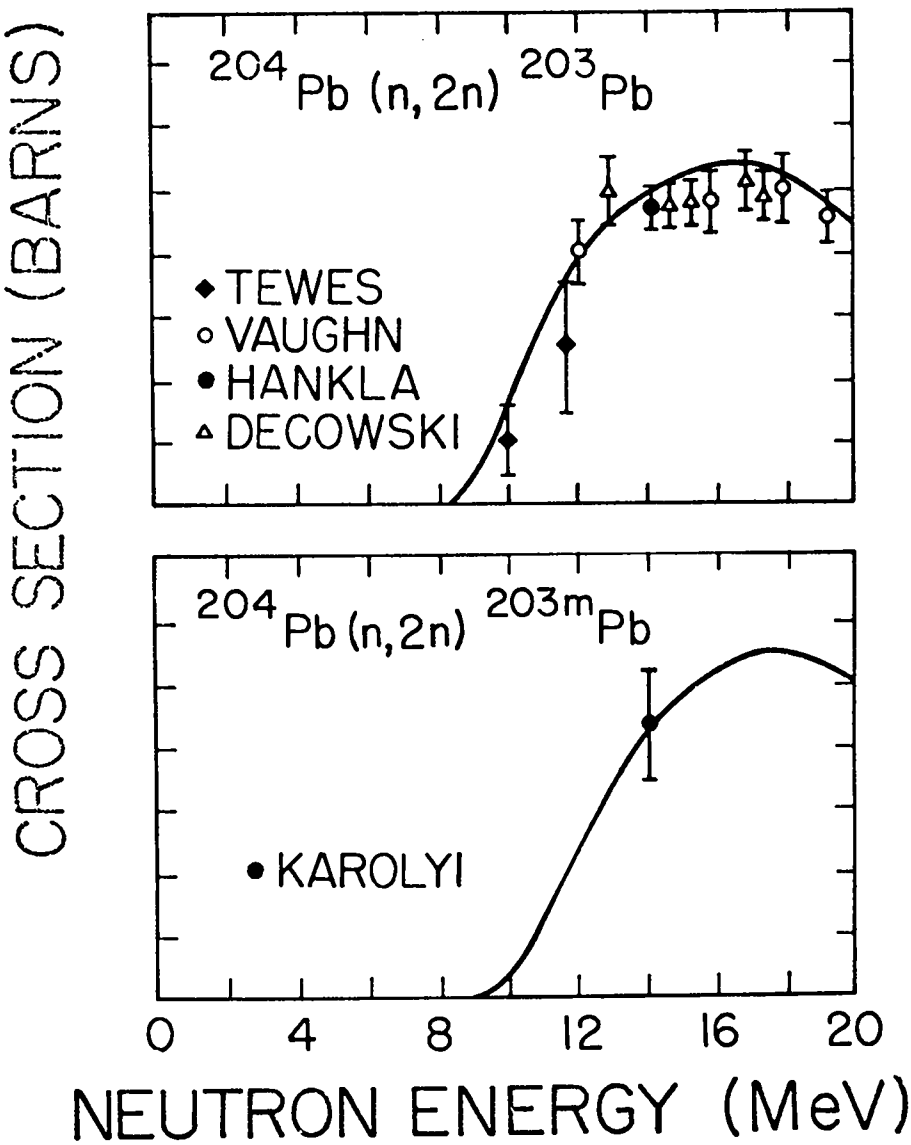

Fig. 11. A comparison of the calculated and experimental values for the total ^{204}Pb(n,2n) cross section, and that part of the ^{204}Pb(n,2n) cross section leading to the 0.85-MeV isomeric state in ^{203}Pb.

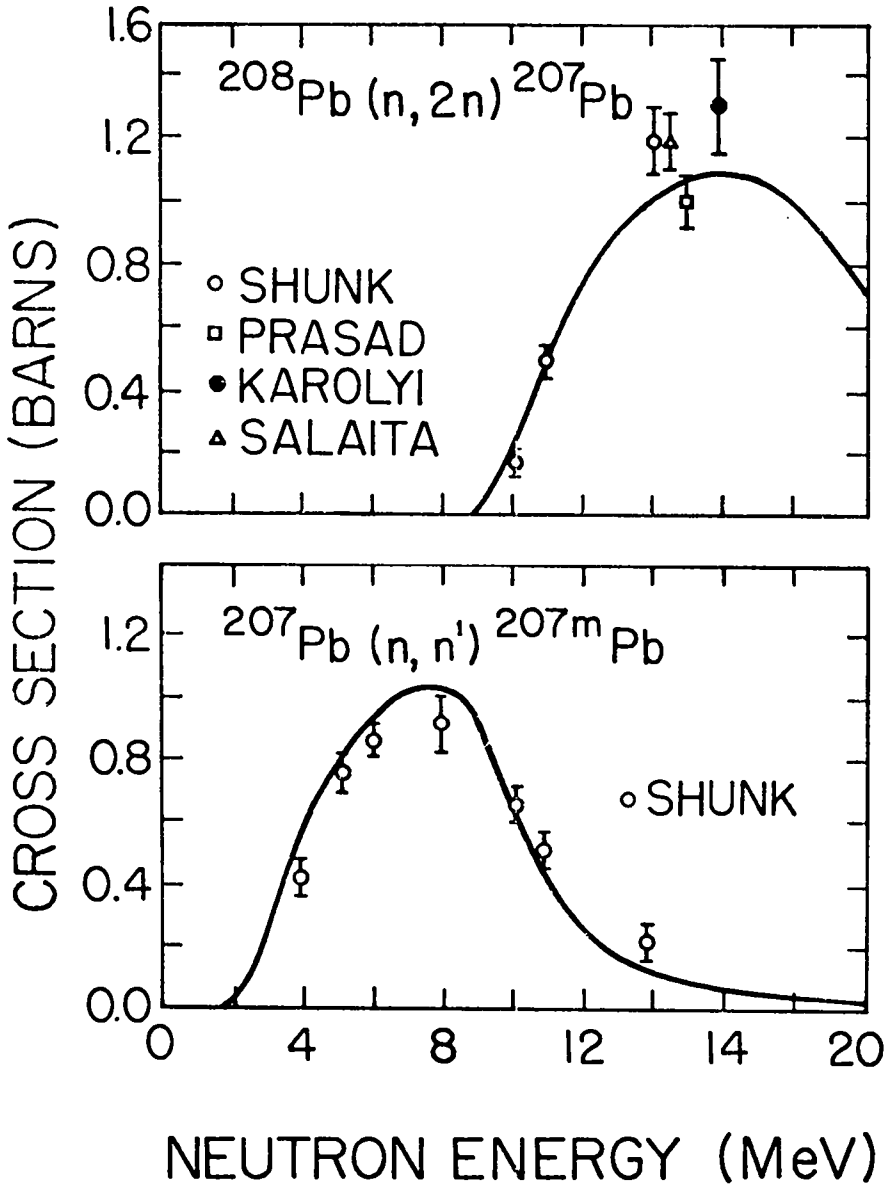

Fig. 12. Calculated and experimental values for the $^{208}Pb(n,2n)^{207}Pb$ cross section as well as the production of the 1.63-MeV isomeric level of ^{207}Pb through the $^{207}Pb(n,n')$ reaction.

G. Time-Dependent Radiation from Mixtures of Plutonium Isotopes (D. G. Foster, Jr. and T. R. England)

The applied use of plutonium from reactors, particularly if the plutonium is recycled, leads to a need for data on the time-dependent spectra of neutrons and photons emitted spontaneously by mixtures of these isotopes. It is important to include x-ray emission in the photon spectrum, as was noted last quarter. In evaluating the spectrum of neutrons from spontaneous fission, one must recognize the fact that the emitting nucleus is at a much lower excitation energy than is the case for neutron-induced fission, so that the nuclear temperature and $\bar{\nu}$ are substantially lower than the values familiar from the induced-fission measurements.

We have performed CINDER calculations of the change in these spectra from the time of separation to 100 years later, using two reference mixtures of isotopes[21] representative of the first plutonium-enriched cycle in a pressurized water reactor and of the equilibrium after many cycles. These compositions are given in Table II.

Immediately after separation, most of the photon radiation comes from the decay of ^{238}Pu, even in the first-cycle mixture. The time dependence thereafter is dominated by the decay of ^{241}Pu, which decays almost entirely by beta emission to the ground state of ^{241}Am. The immediate photons result from a 2.45×10^{-5} alpha branch. Within a few weeks, the ^{237}U daughter from the alpha decay comes into secular equilibrium and triples the photon multiplicity per parent alpha decay. The dominant beta-decay branch produces no photons immediately, and does not become important until enough 433-year ^{241}Am has grown in for its decay rate to become appreciable. The ^{241}Am emission dominates the total radiation within 2 years for the first-cycle mixture, but does not exceed the emission following ^{238}Pu decay until the 20th year in the equilibrium mixture. Figure 13 illustrates the effect of ^{241}Am for the two cases. The yield from ^{241}Pu itself and from its ^{237}U daughter are both too small to show in Fig. 13, however.

Figure 14 illustrates the changes in the photon spectrum which accompany these changes in intensity. The hardening of the spectrum is a direct result of the higher average energy of photons emitted by ^{241}Am.

The spectrum of spontaneous-fission neutrons is almost independent of time after separation, since the nuclear temperatures change rather slowly with mass number, and the spectrum is dominated by isotopes (^{238}Pu and ^{240}Pu) which differ by only two in mass number.

TABLE II

ISOTOPIC COMPOSITIONS

Plutonium Isotope	First Cycle	Equi-librium
238	0.015	0.116
239	0.575	0.216
240	0.232	0.173
241	0.130	0.142
242	0.048	0.353

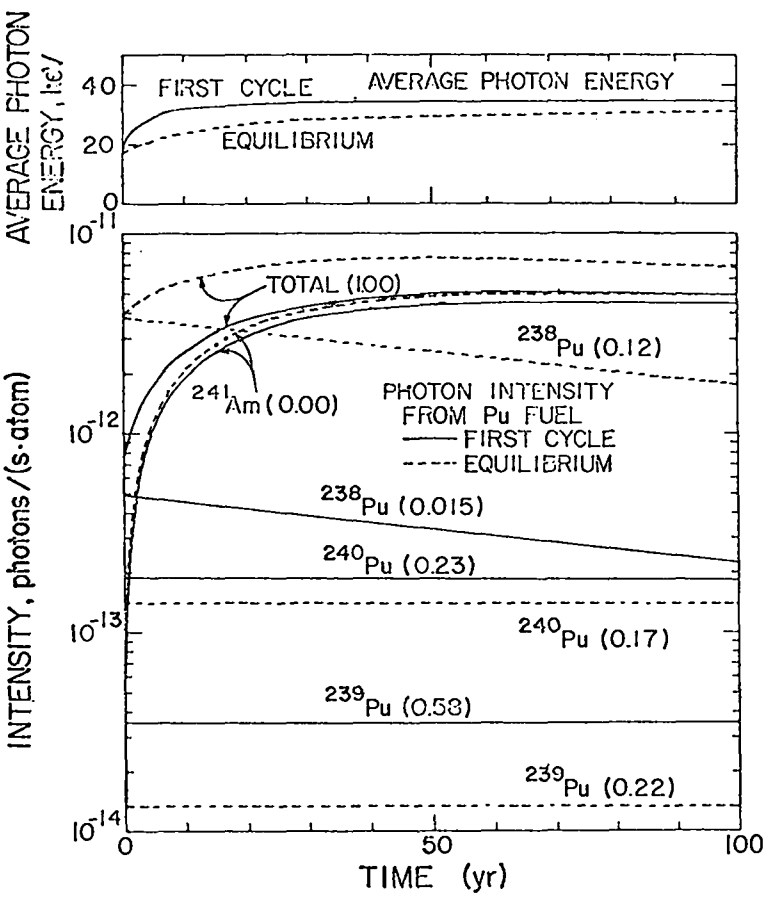

Fig. 13. Absolute photon-emission rates and average photon energies for two different mixtures of plutonium isotopes, calculated from 0 to 100 years after separation. The fraction of each isotope in the initial mixture is given in parentheses after the isotopic symbol. ^{241}Pu, its ^{237}U daughter, and ^{242}Pu have yields too small to show in this figure.

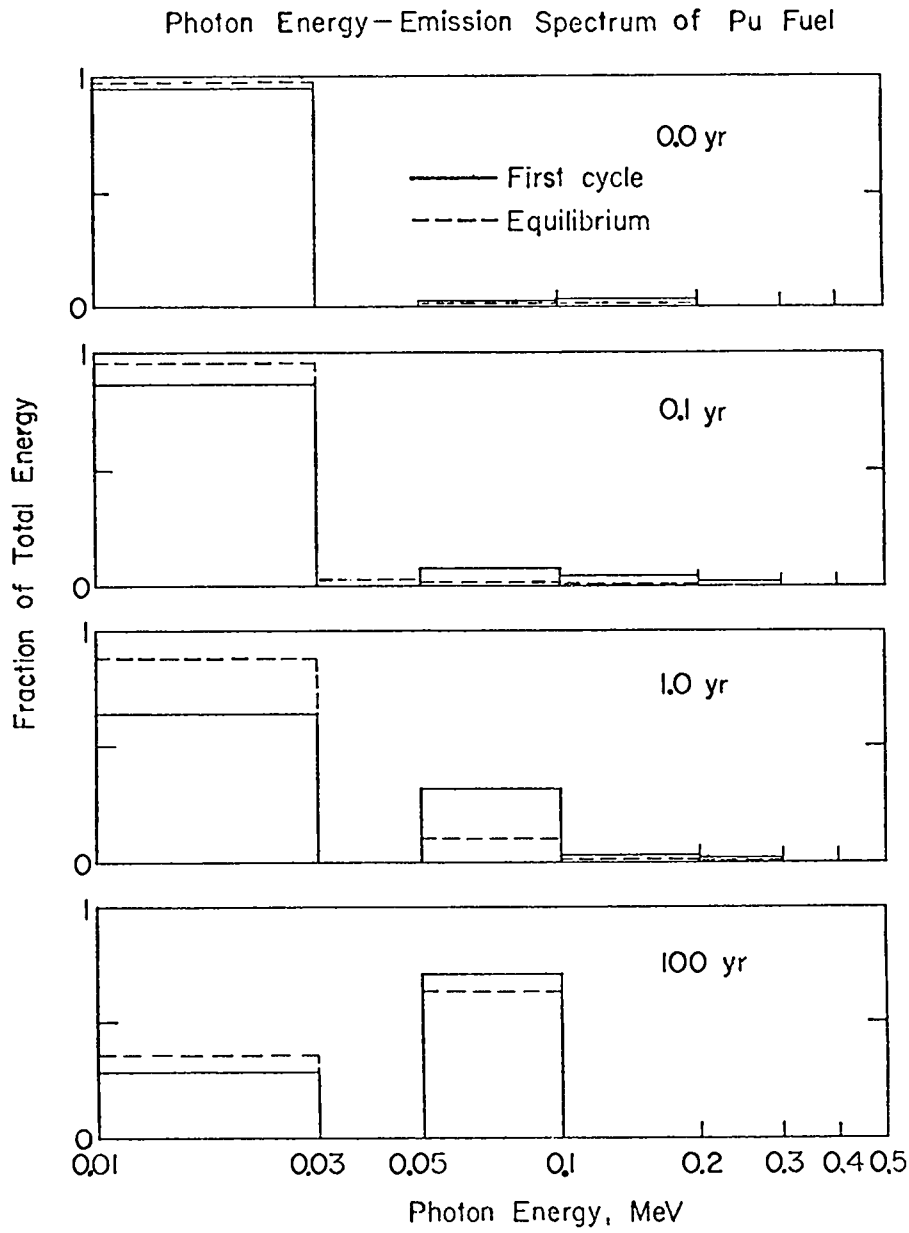

Fig. 14. Normalized energy-emission spectrum as a function of time for two different mixtures of plutonium isotopes. At the time of separation the spectrum is dominated by L x rays. The hardening of the spectrum at later times is caused by the growing in of ^{241}Am.

Table III gives the relevant parameters for each isotope, and Fig. 15 illustrates the time variation of the total emission. The total neutron yield of the equilibrium mixture at separation time is almost double that of the first-cycle mixture because of the much greater ^{238}Pu content, but it decays faster with time because of the short half-life of ^{238}Pu.

H. CSEWG Standards Task Force Meeting at Brookhaven National Laboratory March 22-23 (G. Hale and L. Stewart)

1. The LASL evaluation for hydrogen scattering and for the $^{3}He(n,p)$ cross sections were adopted as Version V standards without modification of the data as presented in Version IV, except for a change in the interpolation scheme for hydrogen.

2. The LASL R-matrix predictions described above for the $^{6}Li(n,\alpha)$ and the $^{10}B(n,\alpha_0)$ and $(n,\alpha_1\gamma)$ cross sections were presented and proposed as Version V standards for energies below 150 keV. Error estimates on the ^{6}Li data range from 0.6% at thermal rising to 3% for energies covering the 240-keV resonance.

3. Oak Ridge National Laboratory (ORNL) made presentations on carbon scattering which indicate the need for changes in the angular distributions up to 2 MeV. These were recommended by the Task Force for Version V.

4. Brookhaven National Laboratory (BNL) will renormalize the $Au(n,\gamma)$ experimental data where appropriate to the new Version V recommended standards and present the results at the Cross Section Evaluation Working Group (CSEWG) Standards Subcommittee meeting at BNL in May.

5. Above 200 keV, much work was undertaken by the group on ^{235}U fission, such as renormalization of earlier data and choosing a normalization for relative measurements, and a preliminary point-wise cross-section evaluation was completed. (LASL has been asked to collaborate with BNL on the point-wise data.) Guidelines were written for an evaluation below 200 keV with BNL, ORNL, Aerojet Nuclear Corporation (ANC), and Bettis cooperating. These results are to be presented for review at BNL in May. It is already apparent, however, that ^{235}U fission will decrease significantly over much of the energy range from a few keV to 20 MeV.

6. The evaluation of the thermal constants, except for the $^{6}Li(n,\alpha)$ reaction, has not been completed, and therefore could not be reviewed at this time. This work should be completed by the May CSEWG Meeting and presented at

TABLE III

SPONTANEOUS FISSION PARAMETERS

Isotope	Nu-Bar	Average Energy MeV	Branching Fraction	Half-Life Years
^{238}Pu	1.920	1.819	1.7×10^{-9}	87.74
^{239}Pu	2.050	1.854	4.5×10^{-12}	24370
^{240}Pu	2.154	1.882	4.9×10^{-8}	6536
^{242}Pu	2.440	1.956	5.5×10^{-12}	386700
^{241}Am	2.310	1.923	3.8×10^{-12}	433

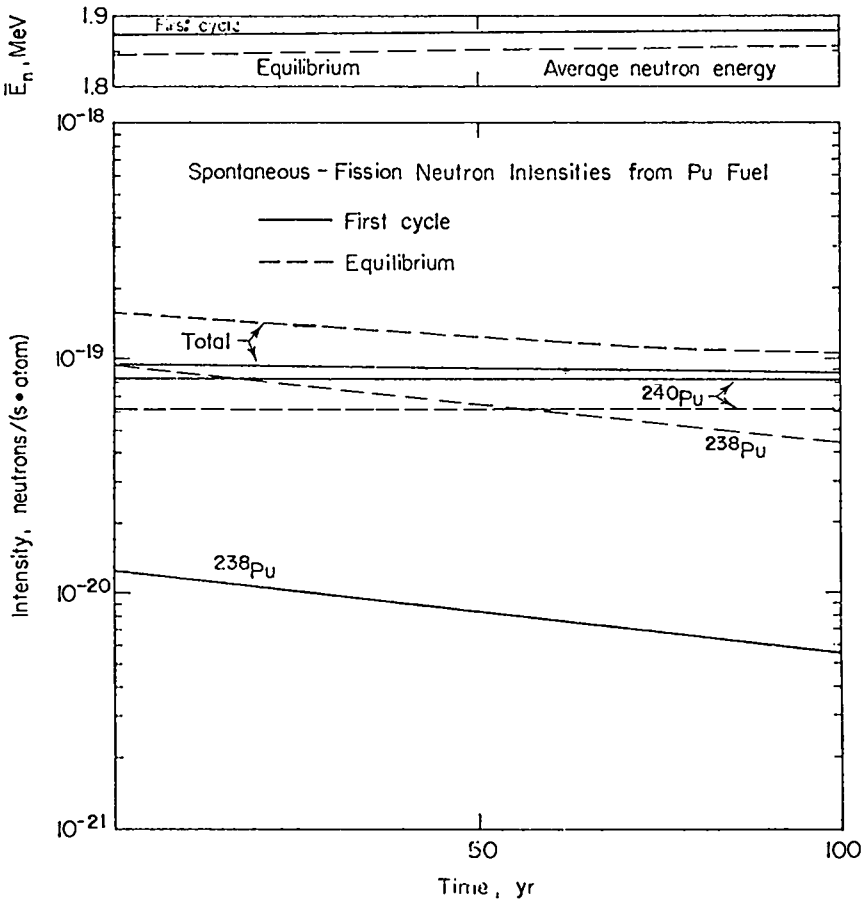

Fig. 15. Absolute emission rate of spontaneous-fission neutrons and the average neutron energies for two different mixtures of plutonium isotopes, calculated from 0 to 100 years after separation.

that time. A preliminary value for ^{235}U fission was made available to the Task Force, however, by Norman Holden (BNL).

I. "Big Three Plus Two" Task Force Meeting at Brookhaven National Laboratory, March 24-25 (R. J. LaBauve and L. Stewart)

The need for changes in the evaluated data for ^{235}U, ^{238}U, ^{239}Pu, ^{240}Pu, and ^{241}Pu was the topic for discussion in this meeting. The energy range covered was sub-thermal to 20 MeV. The topics included changes in thermal constants, $\bar{\nu}$, fission spectrum representation, delayed neutron yields and spectra, in addition to modification of the cross sections themselves. Most of the time was spent on fission and capture with a special session on inelastic scattering and another on sensitivity studies of the important parameters. A format change for the introduction of "pseudo levels" in Version V was proposed by LASL; the formal proposal was completed for early distribution. In concert with BNL, LASL also proposed new Phase I review procedures and helped design the review sheets. This topic will be reviewed at the May meeting by the parent CSEWG Committee.

II. NUCLEAR CROSS-SECTION PROCESSING

A. MINX Code Development (R. E. MacFarlane)

The final draft of the MINX report has been completed except for sections describing IBM conversion and validation of the IBM version against the CDC version. The final CDC version of the code has been sent to ORNL for conversion and testing. When the results of this process are received from ORNL, the MINX report will be completed and the code packages prepared for release to the Argonne Code Center.

B. LIB-IV (R. B. Kidman and R. E. MacFarlane)

Work has been completed on the neutron cross-section portion of LIB-IV, a 50-group, 101-isotope library based on the latest version of ENDF/B-IV. A magnetic tape package containing LIB-IV and the three utilty codes CINX, LINX, and BINX (for manipulating LIB-IV or any CCCC-III data) was sent to BNL for distribution to the nuclear community. Several laboratories have already obtained the package (Westinghouse Advanced Reactor Division [WARD], ORNL, General Electric [GE], and BNL).

This library has been tested in the calculation of several CSEWG benchmark criticals to provide a comparison with other labs and codes and to give an indi-

cation of how LIB-IV may perform in reactor design calculations. Some of the results are shown in Table IV. Only in a few cases do the current LIB-IV results increase the spread in integral results already established by other codes and libraries. Such agreement is encouraging and, since MINX is very similar to ETOX, one can easily extrapolate from past comparisons and validations of ETOX and the shielding factor method (SFM), and state that LIB-IV offers a simple, reliable, accurate, fast, and directly interpretable scheme for processing nuclear data for reactor calculations.

A document describing LIB-IV has also been completed this quarter.[22] Efforts can now focus on the second phase of LIB-IV; that is, adding a library of gamma cross sections that will allow LIB-IV reactor calculations to include gamma-ray effects.

C. 240-Group Library (LIB-IV-240) (R. B. Kidman)

Work was started on generating a 240-group cross-section library based on the data in ENDF/B-IV. These multigroup constants are being stored in the CCCC-III format for use by the nuclear community.

Table V shows the 240-group structure of LIB-IV-240. Many commonly used group structures are subsets of this 240-group structure (for example, the LIB-IV 50-group structure and the widely used 26-group half-lethargy structure). Table VI shows the materials presently comprising LIB-IV-240, their data sources, photostore name, MINX running times, and their sigo sets. All of the materials in Table VI were run for 3 temperatures--300, 900, and 2100 K. All of the materials except ^{238}U were run with the following MINX tolerances: resonance reconstruction 0.005, linearization 0.002, Doppler thinning 0.002, and adaptive integration 0.001. A resonance reconstruction tolerance of 0.01 was used for ^{238}U. The basic, resonance-smoothed weighting function used in MINX was a thermal spectrum (with a Maxwellian temperature of 0.025 eV) up to 0.1 eV, a 1/E spectrum up to 0.8208 MeV, and a fission spectrum (with a nuclear temperature of 1.4 MeV) above 0.9202 MeV. If the ENDF/B-IV data permitted, P_0, P_1, P_2, and P_3 scattering matrices were generated.

Under each material photostore name, there actually exist two files, an ISOTXS and a BRKOXS CCCC-III file for that material. They can be accessed with a CROS control card such as $PHOTOR(FS=LI6L,LOCAL=DUM,OAC=T02RBK,VERS=1) which puts the two ^{6}Li files out on the unit named DUM.

TABLE IV

CENTRAL SPECTRAL INDICES (C/E) AND EIGENVALUES

RATIO W.R.T. U235(N,F)	PU FUELED*			U FUELED*		
	JEZEBEL	VERA-11A	ZPR-6-7	GODIVA	ZPR-3-11	ZPR-6-6A
PU240(N,F)		1.0850			1.0540	
PU239(N,F)	.9363	1.0836	.9625	.9728	.9843	
U238(N,F)	.9485	1.1531	.9377	1.0861	1.0563	.9452
U238(N,G)			1.0534	.9925	.9691	1.0309
NP237(N,F)	.9448	1.1758			1.0506	
U236(N,F)					.7851	
U234(N,F)				.9762	1.0405	
U233(N,F)	.9287	.9993		.9241	.9989	
TH232(N,F)				1.0758		
AU(N,G)				.8491		
KEFF	.9956	.9904	.9893	1.0071	1.0152	.9918
AVE KEFF REF 8	.9922	.9883	.9884	1.0061	1.0091	.9909

*ARRANGED IN ORDER OF SPECTRUM HARDNESS.

TABLE V

LIB-IV-240 GROUP STRUCTURE

I	TOP ENERGY (EV)	LETHARGY WIDTH	I	TOP ENERGY (EV)	LETHARGY WIDTH
1	1.9970E+7	.0167	51	6.0653E+6	.0250
2	1.9640E+7	.0250	52	5.9156E+6	.0250
3	1.9155E+7	.0250	53	5.7695E+6	.0500
4	1.8682E+7	.0250	54	5.4881E+6	.0500
5	1.8221E+7	.0250	55	5.2205E+6	.0500
6	1.7771E+7	.0250	56	4.9659E+6	.0250
7	1.7333E+7	.0250	57	4.8432E+6	.0250
8	1.6905E+7	.0250	58	4.7237E+6	.0250
9	1.6487E+7	.0250	59	4.6070E+6	.0250
10	1.6080E+7	.0250	60	4.4933E+6	.0500
11	1.5683E+7	.0250	61	4.2741E+6	.0500
12	1.5296E+7	.0250	62	4.0657E+6	.0500
13	1.4918E+7	.0250	63	3.8674E+6	.0500
14	1.4550E+7	.0250	64	3.6788E+6	.0500
15	1.4191E+7	.0250	65	3.4994E+6	.0500
16	1.3840E+7	.0250	66	3.3287E+6	.0250
17	1.3499E+7	.0250	67	3.2465E+6	.0250
18	1.3165E+7	.0250	68	3.1664E+6	.0250
19	1.2840E+7	.0250	69	3.0882E+6	.0250
20	1.2523E+7	.0250	70	3.0119E+6	.0500
21	1.2214E+7	.0250	71	2.8650E+6	.0500
22	1.1912E+7	.0250	72	2.7253E+6	.0500
23	1.1618E+7	.0250	73	2.5924E+6	.0500
24	1.1331E+7	.0250	74	2.4660E+6	.0167
25	1.1052E+7	.0250	75	2.4251E+6	.0166
26	1.0779E+7	.0250	76	2.3852E+6	.0084
27	1.0513E+7	.0250	77	2.3653E+6	.0083
28	1.0253E+7	.0250	78	2.3457E+6	.0167
29	1.0000E+7	.0250	79	2.3069E+6	.0166
30	9.7531E+6	.0250	80	2.2689E+6	.0167
31	6.5123E+6	.0250	81	2.2313E+6	.0500
32	9.2774E+6	.0250	82	2.1225E+6	.0500
33	9.0484E+6	.0250	83	2.0190E+6	.0250
34	8.8250E+6	.0250	84	1.9691E+6	.0250
35	8.6071E+6	.0250	85	1.9205E+6	.0250
36	8.3946E+6	.0250	86	1.8731E+6	.0250
37	8.1873E+6	.0250	87	1.8268E+6	.0500
38	7.9852E+6	.0250	88	1.7377E+6	.0500
39	7.7880E+6	.0250	89	1.6530E+6	.0250
40	7.5957E+6	.0250	90	1.6122E+6	.0250
41	7.4082E+6	.0250	91	1.5724E+6	.0250
42	7.2253E+6	.0250	92	1.5335E+6	.0250
43	7.0469E+6	.0250	93	1.4957E+6	.0500
44	6.8729E+6	.0250	94	1.4227E+6	.0500
45	6.7032E+6	.0083	95	1.3534E+6	.0500
46	6.6476E+6	.0084	96	1.2873E+6	.0500
47	6.5924E+6	.0083	97	1.2246E+6	.0250
48	6.5377E+6	.0250	98	1.1943E+6	.0250
49	6.3763E+6	.0250	99	1.1648E+6	.0500
50	6.2189E+6	.0250	100	1.1080E+6	.0500

TABLE V (CONT.)

LIB-IV-240 GROUP STRUCTURE

I	TOP ENERGY (EV)	LETHARGY WIDTH	I	TOP ENERGY (EV)	LETHARGY WIDTH
101	1.0540E+6	.0500	151	1.3569E+5	.0500
102	1.0026E+6	.0250	152	1.2907E+5	.0500
103	9.7783E+5	.0167	153	1.2277E+5	.0500
104	9.6164E+5	.0083	154	1.1679E+5	.0500
105	9.5369E+5	.0500	155	1.1109E+5	.1250
106	9.0718E+5	.0500	156	9.8037E+4	.1250
107	8.6294E+5	.0500	157	8.6517E+4	.1250
108	8.2085E+5	.0500	158	7.6351E+4	.1250
109	7.8082E+5	.0500	159	6.7379E+4	.0750
110	7.4274E+5	.0500	160	6.2511E+4	.0500
111	7.0651E+5	.0500	161	5.9462E+4	.0500
112	3.7206E+5	.0500	162	5.6582E+4	.0750
113	6.3928E+5	.0500	163	5.2475E+4	.1250
114	6.0810E+5	.0500	164	4.6309E+4	.1250
115	5.7844E+5	.0500	165	4.0868E+4	.1250
116	5.5023E+5	.0250	166	3.6066E+4	.0250
117	5.3665E+5	.0250	167	3.5175E+4	.0250
118	5.2340E+5	.0250	168	3.4307E+4	.0750
119	5.1047E+5	.0250	169	3.1828E+4	.1250
120	4.9787E+5	.0500	170	2.8088E+4	.0750
121	4.7359E+5	.0500	171	2.6058E+4	.0500
122	4.5049E+5	.0500	172	2.4788E+4	.0250
123	4.2852E+5	.0500	173	2.4176E+4	.0250
124	4.0762E+5	.0500	174	2.3579E+4	.0750
125	3.8774E+5	.0500	175	2.1875E+4	.0250
126	3.6883E+5	.0500	176	2.1335E+4	.1000
127	3.5084E+5	.0500	177	1.9305E+4	.1250
128	3.3373E+5	.0500	178	1.7036E+4	.1250
129	3.1746E+5	.0250	179	1.5034E+4	.1250
130	3.0962E+5	.0250	180	1.3268E+4	.1250
131	3.0197E+5	.0250	181	1.1709E+4	.1250
132	2.9452E+5	.0250	182	1.0666E+4	.1250
133	2.8725E+5	.0250	183	9.1188E+3	.1250
134	2.8015E+5	.0250	184	8.0473E+3	.1250
135	2.7324E+5	.0500	185	7.1017E+3	.1250
136	2.5991E+5	.0500	186	6.2673E+3	.1250
137	2.4724E+5	.0500	187	5.5308E+3	.1000
138	2.3518E+5	.0500	188	5.0045E+3	.1000
139	2.2371E+5	.0500	189	4.5283E+3	.0500
140	2.1280E+5	.0500	190	4.3074E+3	.0500
141	2.0242E+5	.0500	191	4.0973E+3	.1000
142	1.9255E+5	.0500	192	3.7074E+3	.1000
143	1.8316E+5	.0500	193	3.3546E+3	.1000
144	1.7422E+5	.0250	194	3.0354E+3	.0583
145	1.6992E+5	.0250	195	2.8635E+3	.0417
146	1.6573E+5	.0250	196	2.7465E+3	.0500
147	1.6163E+5	.0250	197	2.6126E+3	.0500
148	1.5764E+5	.0500	198	2.4852E+3	.1000
149	1.4996E+5	.0500	199	2.2487E+3	.1000
150	1.4264E+5	.0500	200	2.0347E+3	.1000

TABLE V (CONT.)

LIB-IV-240 GROUP STRUCTURE

I	TOP ENERGY (EV)	LETHARGY WIDTH	I	TOP ENERGY (EV)	LETHARGY WIDTH
201	1.8411E+3	.1000	221	2.9023E+1	.2500
202	1.6659E+3	.0500	222	2.2603E+1	.2500
203	1.5846E+3	.0500	223	1.7603E+1	.2500
204	1.5073E+3	.1000	224	1.3710E+1	.2500
205	1.3639E+3	.1000	225	1.0677E+1	.2500
206	1.2341E+3	.2500	226	8.3153E+0	.2500
207	9.6112E+2	.2500	227	6.4760E+0	.2500
208	7.4852E+2	.2500	228	5.0435E+0	.2500
209	5.8295E+2	.2500	229	3.9279E+0	.2500
210	4.5400E+2	.2500	230	3.0590E+0	.2500
211	3.5358E+2	.2500	231	2.3824E+0	.2500
212	2.7536E+2	.2500	232	1.8554E+0	.2500
213	2.1445E+2	.2500	233	1.4450E+0	.2500
214	1.6702E+2	.2500	234	1.1254E+0	.2500
215	1.3007E+2	.2500	235	8.7642E-1	.0500
216	1.0130E+2	.2500	236	8.3368E-1	.2000
217	7.8893E+1	.2500	237	6.8256E-1	.0880
218	6.1442E+1	.2500	238	6.2506E-1	.1620
219	4.7851E+1	.2500	239	5.3158E-1	.2500
220	3.7267E+1	.2500	240	4.1399E-1	10.6310
				1.0000E-5	

TABLE VI

LIB-IV-240 MATERIALS GENERATED WITH MINX FROM ENDF/B-IV

I	ISOTOPE	ENDF/B VER IV MAT NO	PENDF NAME + VER NO	PENDF TIMING (SEC)	ISOTXS AND BRKOXS NAME + VER NO	ISOTXS AND BROKXS FROM PENDF (SEC)	SIGO SET*
1	H-1	1269	H1P 1	133	H1L 1	612	A
2	H-2	1120	H2P 1	95	H2L 1	395	A
3	H-3	1169	H3P 1	165	H3L 1	767	A
4	HE-3	1146	HE3P 1	102	HE3L 1	279	B
5	HE-4	1270	HE4P 1	118	HE4L 1	451	B
6	LI-6	1271	LI6P 1	157	LI6L 1	667	A
7	LI-7	1272	LI7P 1	159	LI7L 1	733	A
8	BE-9	1289	BE9P 3	516	BE9L 1	4363	A
9	B-10	1273	B10P 3	428	B10L 1	1095	C
10	B-11	1160	B11P 5	182	B11L 1	466	D
11	C-12	1274	C12P 4	156	C12L 1	420	F
12	N-14	1275	N14P 1	593	N14L 1	1257	A
13	O-16	1276	O16P 1	590	O16L 1	1096	F
14	NA-23	1156	NA23P 2	667	NA23L 1	981	E
15	AL-27	1193	AL27P 2	631	AL27L 1	1155	D
16	FE	1192	FEP 3	1075	FEL 1	1762	F
17	U-235	1261	U235P 2	2832	U235L 1	3212	B
18	U-238	1262	U238P 13	6454	U238L 1	4152	B
19	PU-239	1264	PU239P 2	3505	PU239L 1	3336	F
				18558		27199	

* THE SIGO SETS ARE (IN BARNS):
SET A = 1000, 100, 10, 1, .1, .01
SET B = 10000, 1000, 100, 10, 1, .1
SET C = 1000, 100, 10, 1
SET D = 100000, 10000, 1000, 100, 10, 1
SET E = 1000, 100, 10, 1, .1
SET F = 10000, 1000, 100, 10, 1

As the need arises, more materials will be added to LIB-IV-240 in order to provide a complete library for use in fine-group nuclear calculations.

D. CINX, LINX, BINX (R. B. Kidman and R. E. MacFarlane)

The following utility codes for manipulating CCCC-III ISOTXS, BRKOXS, and DLAYXS files have been completed and documented this quarter. CINX[23] will exactly collapse fine-group data to subset coarse-group structure, and also change the format of the data to 1DX or PERT-V form, if desired. LINX[24] will combine two multi-isotope CCCC-III files into a new composite CCCC-C file. BINX[24] will convert CCCC-III data from binary to BCD mode, or vice-versa, and selectively print the contents of the files.

These three codes are being included in the magnetic tape distribution of LIB-IV.

E. ETOX vs MINX Comparison (R. B. Kidman)

In an effort to discover any remaining errors in MINX, ETOX and MINX results are being thoroughly examined by a detailed group-by-group cross-section comparison, and by comparing effective cross sections and integral results on the Processing Code Comparison Subcommittee's infinite homogeneous ZPR-6-7 specification. Several discrepancies have been discovered that lead to cross-section differences but which seem to have nearly an insignificant effect on k_{eff}.

1. ETOX does not correctly combine f-factor contributions in an overlap group that contains a boundary between a smooth, resolved, or unresolved region.

2. ETOX is not totally correct in its method of handling discrete inelastic scattering.

3. ETOX does not handle the File 5, LF = 1 secondary energy distribution correctly.

4. ETOX arbitrarily resets resonance region f-factors > 1.0 back to 1.0.

5. The MINX and ETOX fission spectrum weighting functions do not cut off at the same energy.

6. MINX does not self-shield the (n,α), (n,d), (n,t), etc., reactions.

7. ETOX does not reaction rate weight ν, μ, or ξ.

Most of these discrepancies will be removed so the comparison can continue on a "clean" basis with a better chance of discovering difficult errors.

F. NJOY Development (R. E. MacFarlane and R. M. Boicourt)

New developments for NJOY this quarter have included CCCCR extensions (see Sec. G), photon interaction processing (see Sec. I), free-form input, and code conversion for the LTSS time-sharing system.

Free-form card input is very convenient for any code, but it is almost necessary for codes used on terminal-based systems such as LTSS. A simple free-form input processor has been added to the NJOY utility code. It was designed to be as machine independent as possible, but slight changes in masking statements and in parameters such as the number of bits per computer word may be required on other systems. Hollerith strings are input as "nHstring" or "*string*." All numbers are read as floating point (integers may be fixed by the calling routine later) and can be delimited with blanks or any character not used for some other purpose. The "E" is required for exponential numbers, but may have spaces before it (i.e., .001 or 1 E-3 are all right, but not 1.-3). The "/" is used to terminate an input operation and leaves any unloaded variables unchanged.

The LTSS time-sharing system and the LRLTRAN language have many peculiarities not found in other computer operating systems. This requires some code conversion, but it also provides a good test of the machine-independent coding philosophy followed in the NJOY development program. For example, in NJOY all input/output takes place through utility routines which can be tailored to a particular operating system without requiring changes to the main program. LTSS input/output is most efficient when data is buffered through LCM. Special versions of the utility routines have been developed for this purpose and are being tested.

G. CCCCR Extensions (R. J. Barrett, R. E. MacFarlane, and R. M. Boicourt)

The CCCCR module has been improved and tested in a number of significant ways. Coding which calculates the isotopic fission spectrum (CHISO), the fission yield vector (SNUTOT), and the transport cross section has been completed and tested against hand calculations. Mathematical formulae for these parameters are as follows:

CHISO: $$\chi_g = \frac{S_g}{\sum_g S_g} \quad ,$$

where $$S_g = \sum_{g'} \sigma_{f,g'\to g}\phi_{g'} + \text{DNORM} \times \chi_{d,g} \quad ,$$

and $$\text{DNORM} = \sum_g \nu_{d,g} \times \phi_{d,g} \times \sigma_{f,g} \quad ,$$

ϕ_g refers to the group flux, and

ν_g refers to the group fission yield.

The subscript f stands for fission and d refers to delayed fission neutrons.

SNUTOT: $$\nu_g = \left[\sum_{g'} \sigma_{f,g\to g'} + \nu_d \sigma_{f,g}\right] \Big/ \sigma_{f,g}$$

TRANSPORT XS: $$\ell\sigma_{tr,g} = \ell\sigma_{t,g} - \sum_{g',x} \ell\sigma_{x,g\to g'} \quad ,$$

where ℓ refers to the Legendre order and X refers to the reaction type. The present version of CCCCR calculates only the P-wave (ℓ=1) transport cross sections.

The BRKOXS section is now correctly calculating the transport self-shielding factor, as verified by hand calculations.

The ISONGX file, an experimental file developed for interfacing (n,γ) cross sections, has been improved through the inclusion of a principal cross-section record which includes cross sections for fission, neutron capture, and nonelastic neutron interactions. The purpose for including this information is discussed in Sec. H.

The CCCCR module will now produce multi-isotopic ISOTXS, BRKOXS, DLAYXS, ISONGX, and ISOGXS files using output from the GROUPR and GAMINR modules.

H. Photon Library (R. J. Barrett, R. E. MacFarlane, and R. M. Boicourt)

In February 1976, Group T-2 released a 50-group, 101-isotope library of multigroup neutron constants (LIB-IV) (see Sec. B). As a supplement to this library, a library of N$\to\gamma$ and $\gamma\to\gamma$ cross sections using the same 50-group neu-

tron structure and the Straker[25] 22-group subset of the CSEWG 103-group gamma structure is being produced. Additionally, coding will be developed to assist the user of the photon library in utilizing the photon data in reactor design codes.

The n→γ group-averaged cross sections are produced in the GROUPR module of NJOY, and output in the experimental ISONGX format by the CCCCR module of NJOY. The ISONGX file differs from the n→γ section of ISOGXS in two very important ways. In addition to the total n→γ cross-section matrix found in ISOGXS, there are also matrices for fission-related gamma production and gamma production from neutron capture. This allows the gamma matrix to be self-shielded properly by the design code. Secondly, a neutron-principal-cross-section record has been included in ISONGX. Thus, the code which self-shields the gamma-production data need only have the self-shielded neutron cross sections (not the f-factors) available to it. During this past quarter, the capability of producing a multi-isotope ISONGX file in NJOY was completely debugged and checked against hand calculations.

Photon-interaction (γ→γ) cross sections for 94 isotopes are available in ENDF/B-IV. These data will be processed into multigroup form using the new GAMINR module of NJOY (see Sec. I). The γ→γ cross sections will be output in the CCCC standard ISOGXS format. During this past quarter, the necessary coding to produce an ISOGXS file containing only the photon-principal cross sections and the γ→γ total cross-section matrix (no n→γ or γ→n data) was produced (see Sec. G for additional details). This program has been tested using output from the GAMLEG[26] photon processing code.

The BINX code[24] was developed to perform BCD → BINARY and BINARY → BCD conversions on the ISOTXS, BRKOXS, and DLAYXS standard interface file. For the purpose of exporting the photon library, BINX has been updated to convert ISONGX and ISOGXS files as well.

If the photon library is to be of any use in reactor design problems, the coding necessary to interface the n→γ and γ→γ data with design codes such as 1DX and SPHINX must be developed. The cross sections will have to be self-shielded, zone-averaged, and collapsed into more compact group structures. Several questions are being studied as to how this can best be accomplished. For instance, it is not yet clear whether a separate code should be developed which takes self-shielding factors, zone mixture densities, and zone fluxes from the design

code, or whether the design code should be altered to do the necessary manipulations. This gamma code must produce both coupled sets of neutron and gamma cross sections and separate files for each. The 1DX and SPHINX codes are being studied in an effort to single out the best answers to these and other questions.

I. Photon Interaction Cross Sections (R. E. MacFarlane, R. M. Boicourt, and D. W. Muir)

Photon absorption and scattering cross sections are important for both shielding and heating calculations. At LASL, various versions of GAMLEG[26] have been used to generate these cross sections. However, recent improvements in the ENDF/B photon interaction files[27] have made form factors for coherent and incoherent scattering easily available. Since GAMLEG is not capable of processing these form factors, a new NJOY module has been designed and coded for processing photon-interaction cross sections.

The GAMINR module is based on the data handling and integration schemes developed for the GROUPR module. Photon cross sections are retrieved from a PENDF tape previously prepared using RECONR. The weight function can be constant or read-in as any function representable as an ENDF/B TAB1 record. The multigroup cross sections can then be generated for total, coherent, incoherent, pair production, and photoelectric using a variety of preset group structures or a structure supplied by the user.

In order to calculate the Legendre components of the coherent and incoherent group-to-group transfer matrix, the appropriate "feed functions" must be computed. These functions are $F_{\ell g'}(E)$, the ℓth component of the probability of scattering into group g' from initial energy E. For coherent scattering

$$F^{coh}_{\ell g'}(E) = \frac{\int_{-1}^{1}(1+\mu^2)\,|F(x)|^2 P_\ell(\mu)\,d\mu}{\int_{-1}^{1}(1+\mu^2)\,|F(x)|^2\,d\mu} ,$$

for E in g' (they are zero otherwise). The form factors are tabulated on the ENDF/B tape vs $x = 20.60744(2E/E_0)\sqrt{(1-\mu)/2}$ where E_0 is the electron rest mass

energy of 0.5110034 MeV. The integrations are performed by Lobatto quadrature using panels defined by the x grid of the ENDF/B table. Form factors between grid points are interpolated according to the scheme specified and not by the log-log-quadratic scheme discussed in Ref. 27. For incoherent scattering, the feed functions become

$$F^{inc}_{\ell g'}(E) = \frac{\int_{g'} dE' S(x)\sigma_{KN}(E\to E')P_\ell(\mu)}{\int dE'(x)_{KN}(E\to E')} ,$$

where

$$\mu = 1 + \frac{E_0}{E} - \frac{E_0}{E'} ,$$

$$x = 20.60744(2E/E_0)\sqrt{(1-\mu/2} \times \sqrt{1 + (E^2/E_0^2 + 2E/E_0)(1-\mu)/2}/(1+E[1-\mu]/E_0) ,$$

and

$$\sigma_{KN} = \frac{3\sigma_T E_0^2}{8E^2}\left[\frac{E}{E} + \frac{E'}{E} + 2\left(\frac{E_0}{E} - \frac{E_0}{E'}\right) + \left(\frac{E_0}{E} - \frac{E_0}{E'}\right)^2\right] .$$

Once again, the integrals are performed using Lobatto quadrature on panels defined by the group breaks and x grid. For large enough energies, the effect of the form factor is neglected to speed up the calculation. Heating KERMA factors (Kinetic Energy Release in MAterial) are computed at the same time as the cross sections and transfer matrix elements by defining special feed functions. Coherent scattering does not cause any heating. For incoherent scattering, the feed function is set equal to

$$F^{inc}_{heat}(E) = E - \frac{\int dE'E'S(x)\sigma_{KN}(E\to E')}{\int dE'S(x)\sigma_{KN}(E\to E')} ,$$

for pair production,

$$F_{heat}^{p.p.}(E) = E - 2 \times 0.5110034 \times 10^{6} \quad ,$$

and for photoelectric "capture,"

$$E_{heat}(E) = E \quad .$$

The heating contributions are totaled as they are computed.

The cross sections, matrix elements, and total heating values are written onto an ENDF-like output tape. This tape can be saved or used as input to a formatting module. Coding has been added to the CCCCR module to write out photon-interaction constants as an ISOGXS file.[28] Gamma production and neutron production sections of the file are flagged off. The principle cross sections include the P_0 weighted total and the P_ℓ transport cross sections, but the "source from total decay" is set to zeros. The "total absorption" cross section contains the photoelectric cross section only--the $\gamma 2\gamma$ reaction is not subtracted. This system will be used to produce a library for distribution as a supplement to LIB-IV.[22]

J. Elastic Scattering of Thermal Neutrons in Polycrystalline Materials (R. E. MacFarlane and R. M. Boicourt)

Thermal neutrons have wavelengths commensurate with crystal plane spacings so Bragg scattering effects must be considered. The most important of these effects is the "Bragg cut-off" below which coherent elastic scattering vanishes. A new group of subroutines has been written for NJOY which calculates the coherent and incoherent components of elastic scattering for hexagonal lattices. The methods used are extensions of those developed for the HEXSCAT code.[29]

The coherent part of the elastic scattering from a polycrystalline material is given by[30]

$$\sigma_{el}^{coh}(E' \to E, \mu_0) = \sigma_{coh} \frac{\pi\hbar^2}{4MEV_0} \sum_{\tau \neq 0}^{\tau_M} \frac{N(\tau)}{\tau} e^{-2W_D} \frac{|F|^2}{N} \delta\left(1 - \frac{\hbar^2\tau^2}{4ME} - \mu_0\right) \delta(E-E') \quad (1)$$

Where M is the mass of the scatterer, V_0 is the volume of the unit cell, $N(\tau)$ is the number of reciprocal lattice vectors of length τ, W_D is the Debye-Waller

factor and $|F|^2/N$ is the form factor per atom of the unit cell. All vectors are summed with lengths less than $\tau_M = \sqrt{8ME/\hbar^2}$. The number of these vectors is very large for even moderate energies (e.g., 234 for 0.08 eV in graphite); however, the vectors become so dense at large τ that the sum can be converted to an integral. This is a limited application of the "incoherent approximation." The scattering kernel becomes

$$\sigma_{el}^{coh}(E'\to E,\mu_0) \cong \sigma_{coh}\frac{\pi\hbar^2}{4MEV_0}\sum_{\tau\neq 0}^{\tau_0}\frac{N\tau}{\tau}e^{-2W_D}\frac{|F|^2}{N}$$

$$\times\ \delta(1-\frac{\hbar^2\tau^2}{4ME}\mu_0)\delta(E-E')$$

$$+\ \sigma_{coh}\frac{\hbar^2}{8\pi ME}\int_{\tau_0}^{\tau_M}d\tau\tau e^{-2W_D}\ \delta(1-\frac{\hbar^2\tau^2}{4ME}-\mu_0)\ \delta(E-E')\,, \qquad (2)$$

where $\tau_0 = \sqrt{8ME_0/\hbar^2}$ and E_0 is an arbitrary break point. Finally, the Legendre components of the coherent elastic scattering cross section become

$$\sigma_{el,\ell}^{coh}(E) \cong \sigma_{coh}\frac{\pi^2\hbar^2}{2MEV_0}\sum_{\tau\neq 0}^{\tau<\tau_0}\frac{N\tau}{\tau}\ e^{-W'\tau^2}\ \frac{|F|^2}{N}\ P_\ell(1-\frac{\hbar^2\tau^2}{4ME})$$

$$+\frac{1}{2}\ \sigma_{coh}\int_{-1}^{(1-\frac{2E_0}{E})}d\mu e^{-W''(1-\mu_0)}\ P_\ell(\mu_0)\quad, \qquad (3)$$

for energies greater than E_0. Only the first term is required for lower energies. The incoherent elastic scattering is given by

$$\sigma_{el,\ell}^{inc}(E) = \frac{1}{2}\sigma_{inc}\int_{-1}^{1}d\mu e^{-W''(1-\mu_0)}\ P_\ell(\mu_0)\,. \qquad (4)$$

The summation in Eq. (3) is performed using the methods of HEXSCAT. For increased efficiency, the contributions for each Bragg edge are precomputed and reused at each energy requested. The energies used to describe the cross sections include two points to describe each Bragg edge and additional points chosen adaptively so as to represent all desired Legendre components of the cross section with linear interpolation to some desired tolerance. The resulting grid is very economical.

K. Continuous-Energy Monte Carlo Cross Sections (R. E. MacFarlane)

The MCNR module of NJOY produces pointwise cross sections and probability distributions for energy and angle distributions for neutrons and photons. These constants are written out in an ENDF-like format originally developed for the ETOPL code.[31] However, the LASL continuous-energy Monte Carlo code MCN[32] uses a different format especially constructed for fast data retrieval. A new formatting code, McNJOY, has been developed to carry out this conversion. It was based on the earlier version used with ETOPL, but it was possible to achieve considerable simplification. All heating calculations were removed because the ETOPL-format tapes already contain pointwise heating cross sections produced by HEATR. All binning and coordinate system transformations were removed since these functions are performed by MCNR. Finally, the photon-spectrum coding was changed to reflect the new representation used by NJOY. The data produced by NJOY-McNJOY is now being tested before the system is put into production.

L. Probabilistic Thinning of Large Neutron Cross-Section Libraries for Monte Carlo (D. W. Muir and R. E. MacFarlane)

Straightforward approaches to the generation of tabular cross-section libraries[33] for use with continuous-energy Monte Carlo neutron transport codes often lead to very large data sets. These large data sets (as many as 20 000 energy/cross-section pairs in the resolved resonance range) cannot be used directly in Monte Carlo codes because of storage limitations. We have attempted to remedy this situation by constructing synthetic cross-section structures, which permit the reproduction of most important neutron transport phenomena with a much smaller, i.e., "thinned," data library.

In matching the thinned set to the original, we have required that the probability table[34] for the thinned set provide a best fit (in a least-squares

sense) to the probability table of the original data. The spacing of points in the thinned set is about one-eighth the average lethargy change per collision. In the keV energy range, this spacing permits significant reduction in the size of Monte Carlo libraries, even for the heavy elements. A further advantage of this approach is that probability tables can be constructed for both the resolved and unresolved resonance ranges,[35] so that a single cross-section representation can be used in both ranges.

A thinning program PROTHR, incorporating this probabilistic thinning method, has been developed as a module of the NJOY cross-section processing system.[36] PROTHR has been used to prepare data libraries for calculation of low-energy resonance capture in ^{238}U, using the Los Alamos Monte Carlo code MCN.[32] As a reference set, we have prepared a tabular cross-section file for ^{238}U, based on ENDF/B-IV (MAT 1262), which covers the energy range from 10^{-5} eV to 10^{3} eV. This file contains around 4800 energy points, close to the maximum allowed by the standard version of MCN.

Using PROTHR, a comparison set was prepared which has only 1900 energy points. The method is intended for Monte Carlo applications, but for testing purposes, the GROUPR module of NJOY was used to prepare self-shielded multigroup cross sections from the two files. A comparison of the two sets of multigroup cross sections is shown in Table VII. The agreement between the two sets is generally good. Similar comparisons between a 1400-point set and the 1900-point set show definite evidence of convergence toward the unthinned results. As a second test, the epithermal capture probability was calculated for a heterogeneous lattice consisting of alternating slabs of D_2O (3-cm thickness) and metallic ^{238}U (0.5-cm thickness). An isotropic source of 1-keV neutrons was located at the center of one of the D_2O slabs. The results of the MCN calculations were 0.385 ± 0.005 (4800-point set) and 0.399 ± 0.005 (1900-point set). These first results from PROTHR suggest that tabular cross-section files can be thinned significantly without seriously distorting important neutron transport properties.

M. Leakage Corrections to Self-Shielded Cross Sections (R. B. Kidman, M. Becker [RPI], and R. E. MacFarlane)

The feasibility of modifying space-dependent cross-section generation codes to account for the effect of flux leakage on effective cross sections is investigated for the case of neutron transport in iron and for critical assembly ZPR-III-54.

TABLE VII

MULTIGROUP CAPTURE CROSS SECTIONS FOR ^{238}U
(barns)

Energy Range (eV)	Dilution Factor (barns/absorber atom) Infinite	100	10
1235-454	2.74 (2.69)*	1.36 (1.30)	0.73 (0.67)
454-167	6.71 (7.52)	1.79 (1.70)	0.84 (0.76)
167-61.4	28.0 (24.7)	3.23 (3.13)	1.40 (1.37)
61.4-22.6	42.1 (43.4)	2.83 (2.72)	1.44 (1.41)

*Results calculated from the reference (unthinned) data set given in parentheses.

In the shielding factor method,[37,38] composition dependence for material m and group g, is introduced through the single variable σ_{om}^{g} defined as

$$\sigma_{om}^{g} = \frac{1}{N_m} \sum_{m' \neq m} N_{m'} \sigma_{tm'}^{g} \tag{5}$$

where σ_t is the total microscopic cross section, N is the atom density, and Σ is a summation over all other materials in the composition. If one can visualize neutron leakage from a group as just another material in the composition absorbing neutrons, it is clear that another term should be added to Eq. (5) to accommodate the leakage effects on material m. Three modifications of Eq. (5) have been programmed into 1DX:[39]

1st Method

$$\sigma_{om\ eff}^{g} = \sigma_{om}^{g} + \left| L_z^g / (\phi_z^g V_z N_m) \right| , \tag{6}$$

2nd Method

$$\sigma_{om\ eff}^{g} = \sigma_{om}^{g} + L_z^g / (\phi_z^g V_z N_m) , \tag{7}$$

3rd Method

$$\sigma_{om\ eff}^{g} = \sigma_{om}^{g} + \frac{2}{\pi} \sqrt{\left| L_z^g / (D_z^g \phi_z^g V_z) \right|} \frac{1}{N_m} , \tag{8}$$

where L_z^g is the group g neutron leakage rate from the geometrical zone z containing material M, ϕ_z^g is the zone average flux for group g, V_z is the zone volume, and D_z^g is the zone diffusion coefficient for group g. The first two methods are simply converting zone leakage rates into effective cross sections that can be added to σ_0. The third method is a change based on buckling theory.[40]

These leakage effects have been most visible for nearly pure materials having deep cross-section minima.[41] For this reason, we have chosen to test the above methods on a model of the Rensselaer Polytechnic Institute (RPI) iron transport experiment.[42] The spherical model consists of a black absorber out

to 3.96 cm, a shell source out to 3.97 cm, a void out to 7.63 cm, and 5 equally thick iron zones out to 53.4 cm.

All three methods appear to have converged satisfactorily after only four iterations between the flux and σ_0. Table VIII compares the resulting elastic cross sections, in each of the iron zones, for a few of the groups around iron resonances. In contrast to the unmodified 1DX results, all three methods exhibit space-dependent cross sections. The largest changes occur in the first and fifth iron zones where the leakage is greatest. With respect to the unmodified 1DX results, the third method (buckling theory) yields the largest changes, while the second method gives the smallest changes. Also, the greatest percentage changes occur in the groups containing the large iron resonances. Table IX compares the resulting flux spectra at the surface of the iron sphere. Table IX shows that, as the effective group cross section is increased by leakage, the resulting flux in that group is decreased and there is an overall global softening of the flux spectra.

The same problem was repeated with ten equally thick iron zones with the results shown in Tables X and XI (similar to Tables VIII and IX). Comparing Table X with Table VIII, we note that the smaller zones can have more leakage and therefore can exhibit larger effective elastic cross sections. Also, Table X better defines the maxima and minima that can occur spatially in the effective cross section.

This demonstrates that significant space-dependent leakage effects can be incorporated into such SFM codes as 1DX or SPHINX.[43] We now try such methods on ZPR-III-54 in order to establish such effects on more standard problems and to determine the best correction to make.

ZPR-III-54 was chosen because of its iron reflector and because of its history of low calculated eigenvalues. The results of applying the buckling theory leakage corrections (the third method) are shown in Tables XII and XIII. (This problem used a different group structure, LIB-IV.) The encouraging points are that it appears one does not have to artificially put in extra zones to get the leakage correction effect, and that only one application of the correction is needed (no iterations). The disappointing note is that the buckling theory correction gives only a 1.5% increase in k_{eff}.

TABLE VIII

LEAKAGE CORRECTION EFFECTS ON FE ELASTIC CROSS SECTION (BARNS)
(5-ZONE RPI FE PROBLEM)

GROUP	CORRECTION METHOD	1ST ZONE (7.6 TO 16.8 CM)	2ND ZONE (16.8 TO 25.9 CM)	3RD ZONE (25.9 TO 35.1 CM)	4TH ZONE (35.1 TO 44.2 CM)	5TH ZONE (44.2 TO 53.4 CM)
24	1ST METHOD	1.8183	1.7076	1.6488	1.6060	2.0234
	2ND METHOD	1.5556	1.5556	1.5556	1.6099	2.0246
	3RD METHOD	1.9447	1.8486	1.7522	1.6956	2.0932
	IDX	1.5556	1.5556	1.5556	1.5556	1.5556
25	1ST METHOD	1.8956	1.8332	1.8104	1.7964	2.0889
	2ND METHOD	1.7235	1.7235	1.7235	1.7235	2.0881
	3RD METHOD	2.0259	1.9699	1.9178	1.8737	2.0734
	IDX	1.7235	1.7235	1.7235	1.7235	1.7235
26	1ST METHOD	2.4107	2.3936	2.3886	2.3879	2.4512
	2ND METHOD	2.3768	2.3768	2.3913	2.3855	2.4499
	3RD METHOD	2.4524	2.4255	2.4034	2.4134	2.4860
	IDX	2.3768	2.3768	2.3768	2.3768	2.3768
27	1ST METHOD	2.7450	2.6488	2.5822	2.6142	2.9117
	2ND METHOD	2.5442	2.5442	2.5789	2.6251	2.9093
	3RD METHOD	2.9018	2.8038	2.6717	2.7408	3.0337
	IDX	2.5442	2.5442	2.5442	2.5442	2.5442
28	1ST METHOD	3.6787	3.5403	3.4629	3.3139	4.1202
	2ND METHOD	3.3138	3.3138	3.3138	3.4459	4.1292
	3RD METHOD	4.0519	3.8964	3.6727	3.4945	4.4561
	IDX	3.3138	3.3138	3.3138	3.3138	3.3138
29	1ST METHOD	1.8827	1.8352	1.7990	1.7684	2.0709
	2ND METHOD	1.6951	1.6951	1.6951	1.6951	2.0748
	3RD METHOD	2.0176	1.9688	1.9114	1.8439	2.1540
	IDX	1.6951	1.6951	1.6951	1.6951	1.6951
30	1ST METHOD	2.1853	2.1469	2.0982	2.0694	2.5988
	2ND METHOD	1.9077	1.9077	1.9077	1.9077	2.5967
	3RD METHOD	2.4486	2.3992	2.3265	2.2541	2.7859
	IDX	1.9077	1.9077	1.9077	1.9077	1.9077

TABLE IX

LEAKAGE CORRECTION EFFECTS ON SURFACE FLUX (N/CM2/SEC)
(5-ZONE RPI FE PROBLEM)

GROUP	TOP ENERGY (EV)	ORIGINAL 1DX	3RD METHOD	2ND METHOD	1ST METHOD
1	1.0000E+7	.22393E-10	.22384E-10	.22385E-10	.22385E-10
2	8.8249E+6	.66841E-10	.66773E-10	.66776E-10	.66776E-10
3	7.7880E+6	.37875E-09	.37862E-09	.37864E-09	.37864E-09
4	6.8730E+6	.61035E-09	.60988E-09	.60993E-09	.60993E-09
5	5.3500E+6	.36705E-09	.36645E-09	.36652E-09	.36652E-09
6	4.7230E+6	.55513E-09	.55125E-09	.55190E-09	.55190E-09
7	4.1686E+6	.57119E-09	.56631E-09	.56721E-09	.56721E-09
8	3.6787E+6	.11223E-08	.11078E-08	.11112E-08	.11112E-08
9	3.2460E+6	.13182E-08	.12993E-08	.13015E-08	.13015E-08
10	2.8650E+6	.91345E-08	.85128E-08	.86899E-08	.86899E-08
11	2.2310E+6	.43707E-08	.41721E-08	.42027E-08	.42029E-08
12	1.9690E+6	.18912E-07	.15934E-07	.16671E-07	.16671E-07
13	1.7380E+6	.26637E-07	.21975E-07	.23405E-07	.23377E-07
14	1.5330E+6	.25268E-07	.20510E-07	.20560E-07	.20844E-07
15	1.3530E+6	.16949E-06	.98322E-07	.11534E-06	.11441E-06
16	1.1940E+6	.33832E-06	.22567E-06	.25814E-06	.25461E-06
17	1.0540E+6	.17120E-05	.15263E-05	.16019E-05	.15928E-05
18	8.2080E+5	.27204E-07	.25070E-07	.13827E-07	.18327E-07
19	7.2430E+5	.42671E-05	.20643E-05	.27607E-05	.26483E-05
20	6.3930E+5	.78626E-05	.67541E-05	.75219E-05	.72779E-05
21	5.6420E+5	.40928E-05	.37525E-05	.40384E-05	.39456E-05
22	4.9470E+5	.37304E-05	.29377E-05	.33248E-05	.32518E-05
23	4.3940E+5	.17849E-05	.13917E-05	.15520E-05	.15655E-05
24	3.8770E+5	.22249E-04	.16874E-04	.19475E-04	.18529E-04
25	3.0200E+5	.90698E-05	.84180E-05	.93735E-05	.88912E-05
26	2.6650E+5	.37702E-05	.45799E-05	.46172E-05	.45302E-05
27	2.3520E+5	.49739E-05	.40737E-05	.44175E-05	.44241E-05
28	2.0750E+5	.39330E-05	.28083E-05	.31693E-05	.32962E-05
29	1.8310E+5	.90153E-05	.74637E-05	.82807E-05	.79939E-05
30	1.6160E+5	.13781E-04	.12159E-04	.13826E-04	.13128E-04
31	1.2590E+5	.27398E-05	.42219E-05	.39722E-05	.39394E-05
32	1.1110E+5	.13708E-05	.22528E-05	.20289E-05	.20448E-05
33	9.8030E+4	.72888E-06	.11446E-05	.98724E-06	.10227E-05
34	8.6510E+4	.30440E-05	.27716E-05	.28913E-05	.29009E-05
35	7.6350E+4	.15920E-05	.24778E-05	.22578E-05	.23039E-05
36	6.7380E+4	.10714E-05	.19247E-05	.15978E-05	.16683E-05
37	5.9460E+4	.10179E-05	.18497E-05	.14935E-05	.15803E-05
38	4.6310E+4	.44190E-06	.81361E-06	.64064E-06	.68569E-06
39	4.0850E+4	.27205E-06	.48459E-06	.37862E-06	.40787E-06
40	3.6060E+4	.18617E-06	.35710E-06	.28674E-06	.30381E-06
41	3.1830E+4	.45179E-07	.69346E-07	.47659E-07	.56237E-07
42	2.8090E+4	.22695E-05	.21291E-05	.19851E-05	.20510E-05
43	2.4790E+4	.72580E-05	.13072E-04	.96749E-05	.10729E-04
44	1.9030E+4	.73364E-06	.15209E-05	.10526E-05	.12078E-05
45	1.7030E+4	.47256E-06	.98735E-06	.66711E-06	.77531E-06
46	1.5030E+4	.29884E-06	.62517E-06	.41702E-06	.48810E-06
47	1.3270E+4	.21274E-06	.44458E-06	.29436E-06	.34602E-06
48	1.1710E+4	.13533E-06	.28328E-06	.18663E-06	.21999E-06
49	1.0330E+4	.21353E-05	.42153E-05	.28305E-05	.33457E-05
50	1.0000E+3				

TABLE X

LEAKAGE CORRECTION EFFECTS ON Fe ELASTIC CROSS SECTION (f factors)
(10 ZONE RPI FE PROBLEM)

Group	Infinitely Dilute X-Sec (barns)	Correction Method	1st Zone (7.63 to 12.2 cm)	2nd Zone (12.2 to 16.8 cm)	3rd Zone (12.2 to 21.4 cm)	4th Zone (21.4 to 25.9 cm)	5th Zone (25.9 to 30.5 cm)	6th Zone (30.5 to 35.1 cm)	7th Zone (35.1 to 39.7 cm)	8th Zone (39.7 to 44.2 cm)	9th Zone (44.2 to 48.8 cm)	10th Zone (48.8 to 53.4 cm)
24	3.1503	1st	0.59071	0.56857	0.55037	0.53517	0.52651	0.51977	0.50745	0.51601	0.52274	0.71980
		2nd	0.49379	0.49379	0.49379	0.49379	0.49379	0.49379	0.49379	9.51671	9.52323	0.72012
		3rd	0.62749	0.61018	0.59417	0.58058	0.56491	0.54667	0.51801	0.54843	0.56394	0.71270
		IDX	0.49379	--	--	--	--	--	--	--	--	--
25	3.1205	1st	0.61523	0.60309	0.59271	0.58451	0.58170	0.57918	0.57655	0.57604	0.57617	0.73418
		2nd	0.55233	0.55233	0.55233	0.55233	0.55233	0.55233	0.55233	0.55233	0.55233	0.73401
		3rd	0.65522	0.64569	0.63648	0.62802	0.61974	0.61060	0.60031	0.60423	0.60552	0.73641
		IDX	0.55233	--	—	--	--	--	--	--	—	—
26	2.7253	1st	0.88738	0.88221	0.87931	0.87670	0.87596	0.87685	0.87659	0.87453	0.87823	0.91750
		2nd	0.87214	0.87214	0.87214	0.87214	0.87708	0.87776	0.87658	0.87214	0.87214	0.91696
		3rd	0.90229	0.89772	0.89274	0.88667	0.87907	0.88463	0.88756	0.87987	0.88882	0.92421
		IDX	0.87214	--	--	--	--	--	--	--	--	—
27	3.6478	1st	0.76228	0.74552	0.73159	0.72243	0.71402	0.70349	0.71424	0.71811	0.72017	0.84485
		2nd	0.69747	0.69747	0.69747	0.69747	0.69747	0.71455	0.71849	0.71989	0.71945	0.84433
		3rd	0.80298	0.78909	0.77591	0.76124	0.74435	0.73398	0.74722	0.75541	0.76251	0.86012
		IDX	0.69747	—	--	--	—	—	--	--	--	—
28	6.1554	1st	0.60349	0.59334	0.58141	0.57250	0.56653	0.55834	0.55336	0.55931	0.56675	0.73496
		2nd	0.53836	0.53836	0.53236	0.53836	0.53836	0.53836	0.55223	0.56581	0.57171	0.73621
		3rd	0.66321	0.65380	0.64123	0.62661	0.61090	0.59833	0.58733	0.58256	0.62623	0.77105
		IDX	0.53836	--	--	--	--	--	--	--	—	—
29	3.0709	1st	0.61328	0.61031	0.60223	0.59457	0.58795	0.58395	0.57961	0.57602	0.56826	0.73524
		2nd	0.55198	0.55198	0.55198	0.55198	0.55198	0.55198	0.55198	0.55198	0.55198	0.73630
		3rd	0.66199	0.65427	0.64614	0.63731	0.62774	0.61260	0.61181	0.60517	0.60344	0.73963
		IDX	0.55198	--	—	—	--	--	--	--	--	--
30	4.7464	1st	0.41618	0.46036	0.45602	0.45071	0.44500	0.44112	0.43805	0.43505	0.43258	0.62264
		2nd	0.40192	0.40192	0.40192	0.40192	0.40192	0.40192	0.40192	0.40192	0.40192	0.62240
		3rd	0.51796	0.51544	0.50998	0.50312	0.49544	0.48796	0.48094	0.47254	0.46868	0.63940
		IDX	0.40192	—	—	--	--	--	--	—	--	—

TABLE XI

LEAKAGE CORRECTION EFFECTS ON SURFACE FLUX (N/CM2/SEC)
(10-ZONE RPI FE PROBLEM)

GROUP	TOP ENERGY (EV)	ORIGINAL IDX	3RD METHOD	2ND METHOD	1ST METHOD
1	1.0000E+7	.22395E-10	.22384E-10	.22385E-10	.22385E-10
2	8.8249E+6	.66143E-10	.66073E-10	.66075E-10	.66075E-10
3	7.7880E+6	.37930E-09	.37917E-09	.37919E-09	.37919E-09
4	6.8730E+6	.61358E-09	.61310E-09	.61315E-09	.61315E-09
5	5.5520E+6	.36529E-09	.36270E-09	.36276E-09	.36276E-09
6	4.7230E+6	.55653E-09	.55260E-09	.55322E-09	.55322E-09
7	4.1686E+6	.56313E-09	.55828E-09	.55910E-09	.55910E-09
8	3.6787E+6	.11344E-08	.11194E-08	.11227E-08	.11227E-08
9	3.2460E+6	.12818E-08	.12651E-08	.12658E-08	.12658E-08
10	2.8650E+6	.93045E-08	.86593E-08	.88342E-08	.88331E-08
11	2.2310E+6	.40639E-08	.39057E-08	.39109E-08	.39137E-08
12	1.9690E+6	.19082E-07	.16049E-07	.16732E-07	.16729E-07
13	1.7380E+6	.26979E-07	.22186E-07	.23602E-07	.23575E-07
14	1.5330E+6	.23606E-07	.19184E-07	.19155E-07	.19219E-07
15	1.3530E+6	.16981E-06	.97824E-07	.11360E-06	.11333E-06
16	1.1940E+6	.33489E-06	.22202E-06	.25239E-06	.24999E-06
17	1.0540E+6	.17453E-05	.15802E-05	.16464E-05	.16420E-05
18	8.2080E+5	.11601E-07	.12364E-07	.50688E-08	.70036E-08
19	7.2430E+5	.42358E-05	.20591E-05	.27239E-05	.26194E-05
20	6.3930E+5	.78961E-05	.68144E-05	.76587E-05	.73889E-05
21	5.6420E+5	.40768E-05	.37630E-05	.40437E-05	.39365E-05
22	4.9470E+5	.37673E-05	.30759E-05	.34562E-05	.33728E-05
23	4.3940E+5	.17365E-05	.13736E-05	.15172E-05	.15386E-05
24	3.8770E+5	.22298E-04	.17648E-04	.20234E-04	.19115E-04
25	3.0200E+5	.91144E-05	.86684E-05	.97373E-05	.91377E-05
26	2.6650E+5	.37526E-05	.45789E-05	.46546E-05	.45445E-05
27	2.3520E+5	.49827E-05	.41424E-05	.44424E-05	.45126E-05
28	2.0750E+5	.39138E-05	.28170E-05	.31770E-05	.32970E-05
29	1.8310E+5	.90162E-05	.77750E-05	.87891E-05	.83658E-05
30	1.6160E+5	.13776E-04	.12657E-04	.14394E-04	.13539E-04
31	1.2590E+5	.27085E-05	.41751E-05	.39945E-05	.40097E-05
32	1.1110E+5	.13679E-05	.21825E-05	.19826E-05	.20371E-05
33	9.8030E+4	.68755E-06	.99687E-06	.83175E-06	.88927E-06
34	8.6510E+4	.30625E-05	.27976E-05	.28771E-05	.28660E-05
35	7.6350E+4	.15898E-05	.24918E-05	.23101E-05	.23826E-05
36	6.7380E+4	.10698E-05	.18912E-05	.15674E-05	.16743E-05
37	5.9460E+4	.10179E-05	.17779E-05	.14264E-05	.15490E-05
38	4.6310E+4	.44025E-06	.77349E-06	.60232E-06	.66267E-06
39	4.0850E+4	.26874E-06	.45667E-06	.35336E-06	.39016E-06
40	3.6060E+4	.19832E-06	.37201E-06	.29582E-06	.32456E-06
41	3.1830E+4	.32275E-07	.25585E-07	.10156E-07	.14806E-07
42	2.8090E+4	.22675E-05	.20717E-05	.18699E-05	.19174E-05
43	2.4790E+4	.72568E-05	.12737E-04	.94186E-05	.10639E-04
44	1.9030E+4	.72804E-06	.14485E-05	.98460E-06	.11622E-05
45	1.7030E+4	.47216E-06	.94244E-06	.62260E-06	.74506E-06
46	1.5030E+4	.29899E-06	.59740E-06	.38941E-06	.46915E-06
47	1.3270E+4	.21286E-06	.42520E-06	.27514E-06	.33274E-06
48	1.1710E+4	.13543E-06	.27078E-06	.17442E-06	.21148E-06
49	1.0330E+4	.21384E-05	.40664E-05	.26742E-05	.32374E-05
50	1.0000E+3				

TABLE XII

BUCKLING THEORY LEAKAGE CORRECTION EFFECTS
ON ZPR-III-54 AS A FUNCTION OF NUMBER OF REFLECTOR ZONES

Number of Reflector Zones	Unmodified IDX κ_{eff}	κ_{eff} After 4 Applications of Leakage Corrections	$\Delta\kappa_{eff}$	% of $\Delta\kappa_{eff}$ Obtained After Just One Application of Leakage Corrections
1	0.93222097	0.94678948	0.01456851	98.69
2	0.93266139	0.94645452	0.01379313	100.80
3	0.93290265	0.94650566	0.01360301	99.92
4	0.93307022	0.94638714	0.01331692	95.54
5	0.93315493	0.94596153	0.01280660	97.32

TABLE XIII

BUCKLING THEORY LEAKAGE CORRECTION EFFECTS ON
ZPR-III-54 SURFACE FLUX ($N/cm^2/SEC$) AS A FUNCTION OF NUMBER OF REFLECTOR ZONES

Group	Top Energy (eV)	Orginal 1-zone IDX	1-zone	After 4 Applications of Buckling Theory Leakage Corrections			
				2-zone	3-zone	4-zone	5-zone
9	3.877+5	0.14035-6	0.12310-5	0.11673-5	0.11905-5	0.12200-5	0.12355-5
10	3.020+5	0.97700-6	0.88960-6	0.88403-6	0.91415-6	0.92036-6	0.93720-6
11	2.352+5	0.69825-6	0.60224-6	0.59393-6	0.60198-6	0.61304-6	0.62432-6
12	1.831+5	0.80702-6	0.70933-6	0.67128-6	0.67769-6	0.69116-6	0.69917-6
13	1.426+5	0.10565-5	0.97378-6	0.10085-5	0.10440-5	0.10726-5	0.10893-5
17	3.183+4	0.47096-6	0.39464-6	0.30747-6	0.30115-6	0.28429-6	0.28260-6
20	2.479+4	0.13751-5	0.14575-5	0.15269-5	0.15539-5	0.15585-5	0.15651-5

N. PRS Flux Weighting Function (R. J. LaBauve, W. R. Wilson, and T. R. England)

We have concluded an investigation of the structure found in the flux spectrum of a mid-life PWR, producing a detailed flux description applicable to the processing of neutron multigroup cross sections for power reactor studies (PRS). The flux weighting function $\phi(E)$, a set of 115 log-log interpolation points as given in Table XIV and shown in Fig. 16, was constructed in the following manner:

1.0×10^{-5} eV - 0.625 eV.

$\phi(E)$ approximates a mid-life PWR thermal spectrum from a 172-group MUFT[44] calculation.

0.625 eV - 3.0×10^{4} eV.

$\phi(E)$ approximates the spectrum from MC^2 (Ref. 45) "ultra-fine" multigroup calculations, using over 2000 energy groups to vividly display the effects of ^{238}U resonances at 6.67, 20.9, 36.7, and 66.0 eV. No attempt was made to represent observed flux depressions of less significance due to resonances of ^{238}U at higher energies.

3.0×10^{4} eV - 1.0×10^{7} eV.

$\phi(E)$ in this region approximates the spectrum from MC^2 "fine" multigroup calculations. The spectrum effects of ^{16}O resonances at 442 keV, 1 and 1.31 MeV, and the ^{16}O window at 2.35 MeV are clearly present. Above 3 MeV $\phi(E)$ assumes the shape of a fission spectrum with a temperature of 1.3427 MeV, approximating the calculated multigroup spectrum.

1.0×10^{7} eV - 2.0×10^{7} eV.

The weighting function in this region is a velocity exponential fusion peak, suggested by D. W. Muir and R. Roussin.[46]

TABLE XIV

PRS FLUX WEIGHTING FUNCTION

POINT	ENERGY, (EV)	FLUX	POINT	ENERGY, (EV)	FLUX
1	1.0000E-05	5.2500E-04	59	3.9900E+05	2.7387E-07
2	9.0000E-03	3.5500E-01	60	4.4200E+05	1.0075E-07
3	1.6000E-02	5.5200E-01	61	4.7400E+05	2.1754E-07
4	2.4000E-02	7.1200E-01	62	5.0200E+05	2.6333E-07
5	2.9000E-02	7.8500E-01	63	5.4000E+05	3.0501E-07
6	3.3000E-02	8.2900E-01	64	6.5000E+05	2.9093E-07
7	4.3000E-02	8.9800E-01	65	7.7000E+05	2.5005E-07
8	5.0000E-02	9.1800E-01	66	9.0000E+05	2.1479E-07
9	5.4000E-02	9.2100E-01	67	9.4100E+05	1.7861E-07
10	5.9000E-02	9.1800E-01	68	1.0000E+06	9.1595E-08
11	7.0000E-02	8.9200E-01	69	1.0500E+06	1.1518E-07
12	9.0300E-02	7.9900E-01	70	1.1200E+06	1.3648E-07
13	1.1200E-01	6.8600E-01	71	1.1900E+06	1.5479E-07
14	1.4000E-01	5.2000E-01	72	1.2100E+06	1.5022E-07
15	1.7000E-01	3.8300E-01	73	1.3100E+06	6.8696E-08
16	2.1000E-01	2.5200E-01	74	1.4000E+06	1.2182E-07
17	3.0000E-01	1.0800E-01	75	2.2200E+06	5.9933E-08
18	4.0000E-01	6.8700E-02	76	2.3500E+06	9.1595E-08
19	4.9000E-01	5.1000E-02	77	2.6300E+06	3.9981E-08
20	5.7030E-01	4.3700E-02	78	3.0000E+06	3.1142E-08
21	6.0000E-01	4.1300E-02	79	4.0000E+06	1.7073E-08
22	1.0000E+00	2.4910E-02	80	5.0000E+06	9.0679E-09
23	1.3518E+00	1.8502E-02	81	6.0000E+06	4.7153E-09
24	4.0100E+00	6.3200E-03	82	8.0000E+06	1.2276E-09
25	5.5047E+00	4.6164E-03	83	1.0000E+07	3.0953E-10
26	5.8842E+00	4.1950E-03	84	1.2570E+07	2.4619E-10
27	6.1350E+00	3.7279E-03	85	1.2600E+07	3.4731E-10
28	6.4490E+00	1.6521E-03	86	1.2700E+07	1.0357E-09
29	6.6700E+00	5.3125E-05	87	1.2800E+07	2.8436E-09
30	6.8940E+00	1.7632E-03	88	1.2900E+07	7.1910E-09
31	7.0100E+00	2.9219E-03	89	1.3000E+07	1.6776E-08
32	7.3080E+00	3.6062E-03	90	1.3100E+07	3.6122E-08
33	1.7530E+01	1.7156E-03	91	1.3200E+07	7.1864E-08
34	1.9860E+01	1.3858E-03	92	1.3300E+07	1.3222E-07
35	2.0370E+01	1.0973E-03	93	1.3400E+07	2.2511E-07
36	2.0900E+01	1.3739E-05	94	1.3500E+07	3.5512E-07
37	2.1400E+01	1.0588E-03	95	1.3600E+07	5.1946E-07
38	2.2500E+01	1.3565E-03	96	1.3700E+07	7.0478E-07
39	3.4000E+01	8.1519E-04	97	1.3800E+07	8.8825E-07
40	3.5600E+01	7.4897E-04	98	1.3900E+07	1.0408E-06
41	3.5900E+01	6.7872E-04	99	1.4070E+07	1.1542E-06
42	3.6700E+01	9.1595E-06	100	1.4200E+07	1.0870E-06
43	3.7400E+01	6.5453E-04	101	1.4300E+07	9.5757E-07
44	3.8700E+01	8.2618E-04	102	1.4400E+07	7.8744E-07
45	6.1200E+01	5.5873E-04	103	1.4500E+07	6.0403E-07
46	6.4930E+01	4.8263E-04	104	1.4600E+07	4.3317E-07
47	6.6000E+01	4.5797E-05	105	1.4700E+07	2.9341E-07
48	6.7100E+01	4.7226E-04	106	1.4800E+07	1.8213E-07
49	6.8200E+01	4.8362E-04	107	1.4900E+07	1.0699E-07
50	1.0100E+03	3.7829E-05	108	1.5000E+07	5.8832E-08
51	2.0000E+04	2.2257E-06	109	1.5100E+07	3.0354E-08
52	3.0700E+04	1.5571E-06	110	1.5200E+07	1.4687E-08
53	6.0700E+04	9.1595E-07	111	1.5300E+07	6.6688E-09
54	1.2000E+05	5.7930E-07	112	1.5400E+07	2.8450E-09
55	2.0100E+05	4.3645E-07	113	1.5500E+07	1.1006E-09
56	2.8300E+05	3.8309E-07	114	1.5676E+07	1.9780E-10
57	3.5600E+05	3.6926E-07	115	2.0000E+07	1.5477E-10
58	3.7700E+05	3.4027E-07			

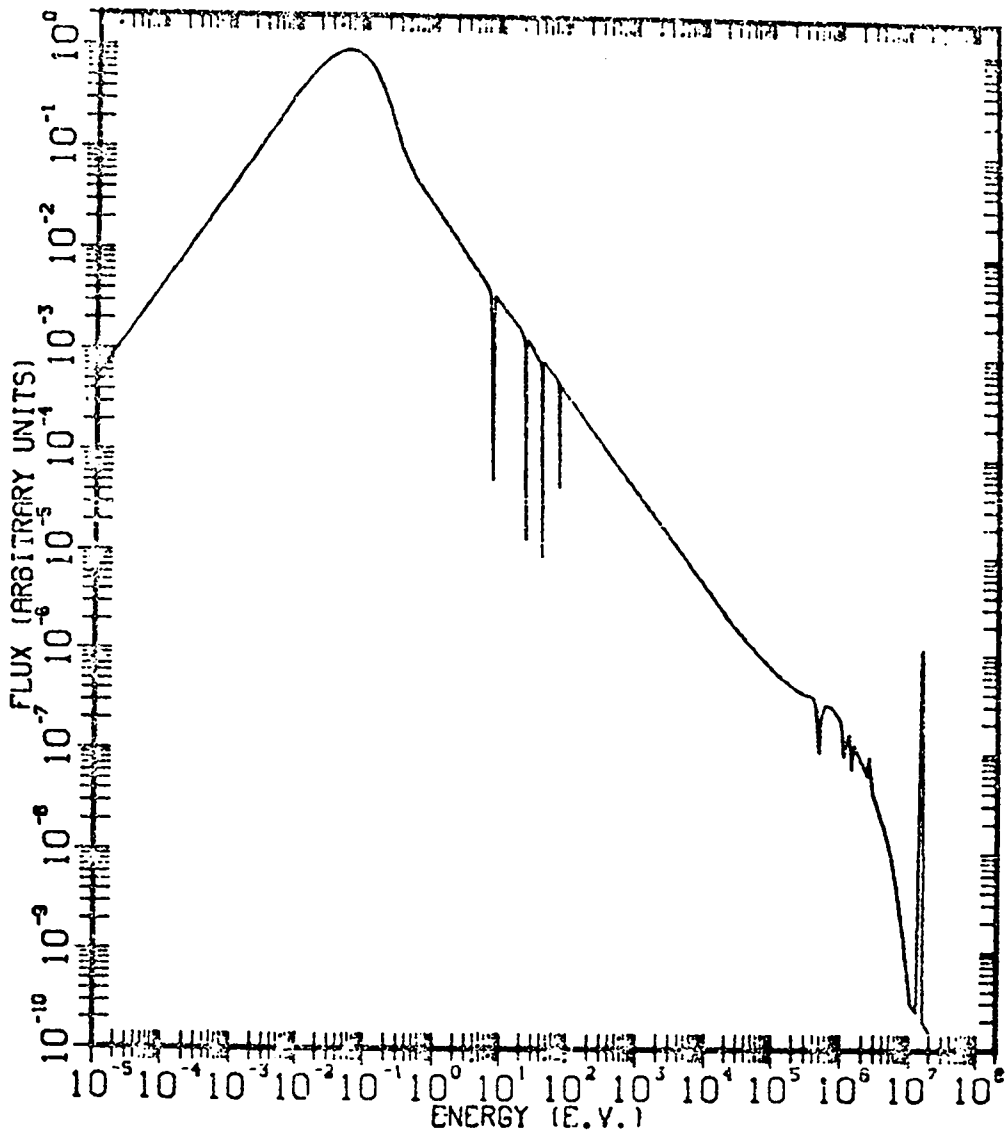

Fig. 16. PRS Flux weighting function.

The PRS flux weighting function is currently used in the NJOY[47] code for processing ENDF/B-IV fission-product absorption cross sections for the CINDER absorption chain library described in Sec. V-C.

III. CROSS SECTIONS FOR HTGR SAFETY RESEARCH

A. HTGR Double-Heterogeneity Space Shielding (M. G. Stamatelatos)

A simple method for space shielding cross sections in a doubly heterogeneous HTGR system using rational approximations and collision probability has been developed.

In the Levine formalism[47,48] of space shielding cross sections for a singly heterogeneous configuration (fuel-rod moderator), the heterogeneity correction is in the form of an added "effective" cross-section term σ_e in the flux weighting expression

$$\phi(E) = \frac{1}{\sigma_t + \sigma_0 + \sigma_e} \quad , \tag{9}$$

where

$$\sigma_e = \frac{1}{N_F \bar{\ell}_F \left(\frac{1}{A} + \frac{C}{1-C}\right)} \quad , \tag{10}$$

and

- N_F - absorber atomic density in the fuel rod
- A - Levine factor, typically 1.35 for a cylindrical rod
- C - Dancoff factor of the regular array of fuel rods in the reactor core
- $\bar{\ell}_F$ - mean fuel-rod chordlength

Starting from collision probability concepts and using rational approximations for the escape probability, it can be shown that Eq. (10) can be modified to account for both levels of heterogeneity (grains in the fuel rod and fuel rods in the core) by replacing A with A* where

$$\frac{1}{A^*} = \frac{1}{A} + \frac{\bar{\ell}_0}{\bar{\ell}_F}\left(\frac{1}{a} + \frac{C_0}{1-C_0}\right) \quad , \tag{11}$$

with

$\bar{\ell}_0$ - mean chordlength of a grain, assumed to be spherical

C_0 - Dancoff factor of the grain structure in a fuel rod

a - Levine-like factor for grains, 16/9 for a sphere.

The Dancoff factor C_0 was calculated in terms of the Sauer chordlength distribution in a cylinder[49]

$$C = \frac{\Sigma_g}{\Sigma_f}\left[1 - \left(1 + \frac{\Sigma_f \bar{\ell}_F}{4.58}\right)^{-4.58}\right] \quad , \tag{12}$$

where

$$\Sigma_g = f_0/\bar{\ell}_0 \quad , \tag{13}$$

$$\Sigma_f = \Sigma_g + \Sigma_1 \quad , \tag{14}$$

and

f_0 - grains volume fraction in a fuel rod

Σ_1 - macroscopic cross section of the fuel rod moderator outside the grains.

The present method was incorporated in a modified version of the 1DX code[39] and was seen to produce results in good agreement (within ~2%) with more detailed shielding methods discussed in previous progress reports.

B. Cross-Section Processing for Safety Analysis (M. G. Stamatelatos and R. J. LaBauve)

Nine-group cross sections for an end-of-equilibrium-cycle (EOEC) composition were generated at the following core and reflector temperatures: 300, 500, 600, 800, 1000, 1200, 1500, 1700, 2000, 2300, 2600, and 3000 K. The generation procedures as well as the theory involved (double-heterogeneity space shielding, etc.) have previously been discussed and will be incorporated in a forthcoming comprehensive report.

A preliminary examination of important cross sections at three of the temperatures (300, 1200, and 3000 K) has resulted in the following conclusions:

1. There is reasonable overall agreement between the LASL and the General Atomic (GA) cross sections.

2. There is some difference in the space shielding of important resonance absorber cross sections (^{232}Th, ^{233}U, ^{235}U) partially due to the basic input data (the LASL cross sections have used ENDF/B basic data).

3. There does not appear to be a significant or systematic dependence on temperature of the differences between the two sets of cross sections.

4. The LASL cross sections seem to be overall more self-consistent than the GA cross sections (e.g., a few GA group-scattering cross sections are negative or in great disagreement with expected values, possibly due to the cross-section balancing procedure).

5. Differences in the ^{16}O cross sections due to bound (GA) and unbound (LASL) treatments are of small importance.

A comparison of the LASL and the GA absorption cross sections for ^{232}Th at 300, 1200, and 3000 K is made in Table XV.

IV. EFFECT OF DISPERSION MATRIX STRUCTURE ON A DATA ADJUSTMENT AND CONSISTENCY ANALYSIS (W. A. Reupke [Georgia Tech] and D. W. Muir)

In previous contributions,[50-52] a consistent algorithm for the analysis and adjustment of combined differential and integral data was set forth. Application of this technique to thermonuclear neutronics data is in progress and preliminary results have been reported elsewhere.[53] In the present contribution, the effect on these results of correlations in the error matrix of differential data is examined. It is shown that in a specific case, the inclusion of correlated components of error in the differential data does not significantly influence the consistency findings. Although it is expected that in other cases of interest the differential data error matrix will be significant, we present

TABLE XV

^{232}Th Absorption Cross Sections (Barns) at 300, 1200 and 3000 K

Gp. No.	Energy Boundaries	300 K		1200 K		3000 K	
		LASL	GA	LASL	GA	LASL	GA
1	10 MeV - 183 KeV	0.1647	0.1755	0.1647	0.1755	0.1647	0.1755
2	183 KeV - 961 eV	0.8173	0.8889	0.8383	0.9070	0.8506	0.9157
3	961 - 17.6 eV	6.6174	7.2010	8.5036	9.3061	10.036	10.988
4	17.6 - 3.95 eV	0.1415	0.1392	0.1419	0.1392	0.1423	0.1398
5	3.95 - 2.38 eV	0.2963	0.2958	0.2964	0.2959	0.2966	0.2972
6	2.38 - 0.414 eV	0.9403	0.9080	1.1276	1.0711	1.0843	1.0650
7	0.414 - 0.1 eV	2.7533	2.6911	2.5021	2.4312	2.2502	2.2133
8	0.1 - 0.04 eV	4.6475	4.4992	4.3990	4.3266	4.3319	4.2815
9	0.04 - 10^{-5} eV	8.2410	7.8466	7.9300	7.6734	7.8258	7.6211

these results to illustrate alternatives which are available before completion of the more costly and systematic evaluations of differential data error files.

As described in Ref. 53, the consistency analysis compared calculated[54] and measured[55] values of 11 radial tritium production measurements obtained in a lithium deuteride sphere driven by a central 14-MeV neutron source. Combined fitting of the integral data with a 17-energy-group representation of the $^{7}Li(n,n')\alpha T$ tritium production reaction required an estimate of the relative uncertainties in these data, as contained in a dispersion matrix of order 28. The structure of this matrix is block diagonal, and consists of a differential data submatrix of order 17 and an integral data submatrix of order 11. No initial correlations are allowed between differential data as a type and integral data as a type.

Since the correlated errors for evaluated ^{7}Li cross sections have not been estimated, the structure of the submatrix of multigroup differential data was varied from zero correlation to full positive correlation (for all elements) to test the effect of correlation strength on the consistency analysis.[56] A generalization of the program COVMAT was used to generate the required matrices.[57] The DAFT3 subroutine of ALVIN was used to circumvent inversion of the full differential and integral data dispersion matrix; in DAFT3, the singular differential data dispersion matrix was separated and transformed to an invertable matrix.

The structure of the submatrix of integral data uncertainies was inferred from estimates of correlated and uncorrelated radial production uncertainties given in Ref. 55. This submatrix implied ~3% uncertainty in the volume-integrated production, in contrast to the reported[55] value of 10% which included a qualitative estimate of additional--but unidentified--sources of error. Since the degree of correlation of these additional sources of error also was not estimated in Ref. 55, a "high pattern" matrix, assuming full correlation amongst the additional sources, was considered in order to set an upper bound on the χ^2 of the published data. Since the resultant dispersion matrix of integral data was nearly singular, tests on similar matrices and matrix identity checks were used to validate the required inversion of this matrix by the DAFT3 module in ALVIN.

The effect of the alternate differential data dispersion matrices on the consistency of the combined differential and integral data, as measured by the

χ^2 per degree of freedom, is shown in Table XVI for the "high-pattern" integral data correlation matrix.

A smooth variation between the above values of final χ^2 (or χ^2 after fitting) is observed for differential data correlation strengths ranging between the extremes listed above.

From inspection of Table XVI, it is apparent that the initial χ^2 is unaffected by the correlation changes. This result is a natural consequence of the fact that the correlated contributions to the initial χ^2 all contain the elements of the initial discrepancy vector of differential data and these discrepancies are identically zero when the variables are linearized about a point corresponding to the initial differential data, as is done in ALVIN.

A stronger and less obvious result is that the final consistency is not greatly dependent on the assumed structure in the differential data dispersion matrix. Numerical experiments with integral data dispersion matrices other than the "high pattern" indicate a similar weak dependence on differential data correlation strength. In particular, similar results are expected for more realistic integral data dispersion matrices and at lower values of final χ^2. Not indicated in the table is the detailed pattern of the adjustments achieved in the fit. As expected, the pattern of adjusted values is markedly sensitive to the assumed differential data correlation strength.

Our calculations thus establish that an application of consistency analysis to the ^{n}LiD integral experiment is relatively insensitive to the detailed correlation pattern of the ^{7}Li(n,n')αT multigroup error matrix. We also indicate a technique supplemental to the detailed evaluation of cross-section error matrices. Because this detailed evaluation process may consume significant resources in other consistency problems of interest, we believe it is useful to establish

TABLE XVI

EFFECT OF ALTERNATE DIFFERENTIAL DATA DISPERSION MATRICES ON THE CONSISTENCY OF THE COMBINED DIFFERENTIAL AND INTEGRAL DATA

^{7}Li(n,n')αT Matrix 15% Std. Error	χ^2/DOF, Initial	χ^2/DOF, Final
Uncorrelated (ρ=0)	8.7	5.2
Fully correlated (ρ=1)	8.7	6.0

in a more general manner the conditions which determine the effect of dispersion matrix structure on consistency analysis.

V. FISSION PRODUCT AND DECAY DATA STUDIES

A. Fission Yield Theory (D. G. Madland and T. R. England)

Efforts on fission yield theory have been directed into two areas. The first area is that of the currently used phenomenological yield model.[58-60] Improvements have been sought in the values of certain model parameters and in the description of certain existing empirical relationships. A study of one class of phenomena has led to the introduction of a new model relationship. This work has received greater priority during the quarter because of pending deadlines for the ENDF/B-V fission product evaluated nuclear data file (23 data sets with ~ 1000 independent yields per set). The second area is that of the development of a fundamental yield theory to be applied to new regions (and new energies) which are devoid of data and, consequently, where the phenomenological model is of questionable merit.

1. Phenomenological Model

Studies have been made of the dependence of the most probable charge and charge distribution width, and the magnitude of the even-odd Z effect, upon incident neutron energy and fissile nuclide. With respect to the later effect, correlations among excitation energy of the compound system, fission barrier height, and an averaged pairing energy seem promising. It may be possible to parameterize the magnitude of the even-odd Z effect (and even-odd N effect) in terms of these known quantities so long as the constraint of an "averaged" pairing energy is not too harsh. Initial calculations have indicated a reasonable correlation with the available data.

A model of the distribution of independent yield strength between isomers has been developed, calculated, and tested successfully against the existing data.[61] The model employs the angular momentum distribution form of Rasmussen, has one parameter (an effective energy-dependent fragment angular momentum), and requires knowledge of the angular momenta of the involved isomeric states. A catalog file (≈160 cases) of isomeric branching has been constructed for inclusion in ENDF/B-V.

2. Fundamental Yield Theory

Work has begun on a more soundly based yield theory. Although much progress has been made in fission theory,[62] no clear direction has yet evolved

for the treatment of yields. From a pragmatic standpoint, the most reasonable method seems to be a statistical model which employs the liquid drop formalism to describe the collective coordinates. Intentions are to begin within this framework by calculating mass, charge, and kinetic energy distributions as functions of fissile nuclide and incident neutron energy. As much latitude as is possible will be built into the calculations in order to accomodate new developments. This work will begin in earnest following the modifications of the phenomenological yield model for ENDF/B-V.

B. Method for Calculating Average Beta Energies and Beta Spectral Shapes (M. G. Stamatelatos and T. R. England)

Presented here is a new efficient method for calculating average beta energies and beta spectral shapes for allowed and forbidden unique transitions of the first, second, and third type. This method is especially useful and economical for calculating average beta energies and beta spectra for the large number of fission-product radionuclides. We have found that application of this method to the ENDF/B-IV fission products reduces the computational time by more than an order of magnitude over the Fermi method,[63,64] which requires numerical integration and complex gamma function calculations. Our method is accurate over the entire range of Z values, and especially useful for the occasional user interested in a few nuclides because it only requires the use of a pocket calculator.

Briefly, the method is as follows. The probability for beta emission with total relativistic energy, in $m_e c^2$ units, between W and W + dW is[63,64]

$$N(W,Z) = C|M|^2 \, F(Z,W) \, K(W) W \sqrt{W^2-1} \, (W_0-W)^2 \quad , \tag{15}$$

where K(W) is 1 for allowed transitions, W_0 is the maximum beta energy, $|M|^2$ is the square modulus of the transition matrix element, and C is a constant. The electron density ratio F(Z,W) is given by a solution to the Dirac equation[63,64]

$$F(Z,W) = \frac{4(1+\frac{s}{2})}{|\Gamma(3+2s)|^2} \left(\frac{2R}{\lambda_c}\right)^{2s} e^{\pi y} (W^2-1)^s \, |(1+s+iy)|^2 \quad , \tag{16}$$

where

$$s = \sqrt{1 - (\alpha Z)^2} - 1, \quad \text{and} \quad y = \alpha Z \frac{W}{\sqrt{W^2-1}} \quad , \tag{17}$$

and α and λ_c are the fine-structure constant and the Compton wavelength, respectively.

We have attempted numerous ways to approximate F(Z,W), or portions thereof, with simple, accurate, analytically integrable functions. We have found that the best way is to approximate

$$F(Z,W)\ \sqrt{W^2-1}\left(\frac{2R}{\lambda_c}\right)^{-2s}$$

by a parabola,

$$A_0(Z) + A_1(Z)W + A_2(Z)W^2 \quad ,$$

with coefficients as functions only of the atomic number Z. This approach yields a simple form of N(W,Z) good for the entire range of Z.

When this approximation is inserted into Eq. (15), it can be analytically integrated to calculate the beta spectrum in an arbitrary group structure, the intensity, or the average kinetic energy $\langle W-1 \rangle$. The latter, for an allowed transition, is given by

$$\langle W-1 \rangle = \frac{\sum_{i=0}^{7} B_i W_0^i}{\sum_{i=0}^{6} C_i W_0^i} \quad , \tag{18}$$

where

$$B_0 = \frac{A_0}{20} + \frac{A_1}{30} + \frac{A_2}{42} \quad ; \quad B_1 = -\left(\frac{A_0}{6} + \frac{A_1}{10} + \frac{A_2}{15}\right)$$

$$B_2 = \frac{A_0}{6} + \frac{A_1}{12} + \frac{A_2}{20} \quad ; \quad B_3 = 0$$

$$B_4 = -\frac{A_0}{12} \quad ; \quad B_5 = \frac{A_0 - A_1}{30}$$

$$B_6 = \frac{A_1 - A_2}{60} \quad ; \quad B_7 = \frac{A_2}{105}$$

$$C_0 = -\left(\frac{A_0}{4} + \frac{A_1}{5} + \frac{A_2}{6}\right); \quad C_1 = \frac{2A_0}{3} + \frac{A_1}{2} + \frac{2A_2}{5}$$

$$C_2 = -\left(\frac{A_0}{2} + \frac{A_1}{3} + \frac{A_2}{4}\right); \quad C_3 = 0$$

$$C_4 = \frac{A_0}{12} \quad ; \quad C_5 = \frac{A_1}{30}$$

$$C_6 = \frac{A_0}{60} \quad . \tag{19}$$

In terms of the kinetic energy, Eq. (18) reduces to the ratio of two third-order polynomials.

Analogous expressions exist for forbidden unique transitions. When $A_0(Z)$ and $A_2(Z)$ are set to zero and $A_1(Z)$ set to unity, this expression reduces to a simpler expression [65,66] used for averaging most beta energies in the ENDF/B-IV files.[65] Although the present method is superior to the older expression, we have also tested the older one against Fermi theory calculations using numerical integration of N(W,Z) with F(Z,W) from Eq. (16) and found it good for all fission products to within a few percent (<3%). The present method is not only more accurate for computing the average beta energy of fission products, it also gives very good spectral shapes and average energies for actinides and light elements where the old method is less satisfactory. For example, the average energies for fission products and for Z values through the actinide region are approximated to better than 1%.

For the anticipated expansion of decay data in ENDF/B-V into light and heavy nuclides, this new approximation should be particularly useful.

C. Absorption Chain Library for EPRI (W. B. Wilson, T. R. England, M. G. Stamatelatos, and R. J. LaBauve)

An absorption chain library for an older, modified version of the CINDER code[65] is presently in preparation. This data set describes the 185 significant fission product absorbers and precursors in 77 linear nuclide chains. Infinite dilution capture cross sections are currently being processed from ENDF/B-IV[66] in the PRS-154 group structure[67] using the weighting function described in Sec. II-N.

The NJOY[47] cross-section processing code has replaced the MINX[68] code in processing these multigroup cross sections to minimize computer time and expense. The processed 154-group cross sections are stored on photostore in a format compatible to the collapsing routine TOAFEW, which produces few-group cross sections for the CINDER library. These 154-group cross sections are retained for other applications.

ENDF/B-IV yield data has been processed by the routine YLDECK, describing the fission yield to each of the 185 nuclides of the library from the 10 ENDF/B-IV combinations of fissionable nuclide and incident neutron energy.

The version of CINDER to be supplied to the Electric Power Research Institute (EPRI) is a modification of the version described in Ref. 65. Improvements in roundoff control have been completed, similar to those incorporated into CINDER Version 7.[69] The EPRI code version incorporates a k_{eff} routine for use in survey calculations. It is compatible with FORTRAN II and IV and will compile on any modern computer.

D. Decay Heating, Gas Content, and Spectra Calculations for Fission Products (T. R. England, M. G. Stamatelatos, and N. L. Whittemore)

Several routines have been added to CINDER-10 and the ENDF/B-IV libraries have been extensively checked. Extensive results for noble gas and halogen content and decay heating in ^{235}U fission products were computed and sent to the Nuclear Regulatory Agency. Tables XVII and XVIII give representative results for two extreme cases--a ^{235}U fission burst and "infinite" irradiation at constant power. The latter case is meaningful only when neutron absorption in the fission products is forced to be negligible; then either case can be used to construct the heating rates for finite power histories. If

TABLE XVII

U235 THERMAL FISSION BURST
2/11/76

TIME FOLLOWING BURST (S)	MEV/FISS/S BETA	MEV/FISS/S GAMMA	MEV/FISS/S TOTAL	% IN GAS PRODUCTS — DENSITY — ALL GAS	% IN GAS PRODUCTS — DENSITY — RADIO-ACTIVE GAS	% IN GAS PRODUCTS — ENERGY RATES — BETA	% IN GAS PRODUCTS — ENERGY RATES — GAMMA	% IN GAS PRODUCTS — ENERGY RATES — TOTAL
0.0+0	9.236-1	7.032-1	1.627+0	26.08	25.42	13.46	14.86	14.07
1.0-1	8.044-1	6.084-1	1.413+0	25.98	25.31	14.23	15.69	14.86
5.0-1	5.263-1	3.905-1	9.168-1	25.66	24.96	16.92	18.57	17.63
1.0+0	3.764-1	2.755-1	6.520-1	25.36	24.64	19.06	20.85	19.82
5.0+0	1.331-1	9.411-2	2.273-1	24.12	23.22	21.35	23.77	22.35
1.0+1	7.517-2	5.460-2	1.298-1	23.45	22.37	21.91	24.32	22.92
5.0+1	1.440-2	1.348-2	2.788-2	21.17	18.96	26.23	26.21	26.22
1.0+2	6.554-3	6.514-3	1.307-2	19.77	16.74	25.50	24.11	24.81
5.0+2	9.206-4	9.143-4	1.835-3	16.60	12.27	18.13	15.98	17.06
1.0+3	4.328-4	4.684-4	9.012-4	16.01	11.46	12.02	14.27	13.19
5.0+3	5.852-5	9.157-5	1.501-4	17.53	11.31	17.06	30.26	25.11
1.0+4	2.418-5	3.608-5	6.026-5	18.05	10.39	21.62	44.45	35.29
5.0+4	3.653-6	3.291-6	6.944-6	16.43	7.274	16.84	44.77	30.08
1.0+5	1.238-6	1.362-6	2.600-6	15.38	5.921	24.63	44.53	35.06
5.0+5	1.108-7	2.069-7	3.177-7	14.34	3.374	25.49	42.50	36.57
1.0+6	5.609-8	1.045-7	1.606-7	13.73	1.960	17.57	26.32	23.27
5.0+6	1.037-8	1.281-8	2.318-8	12.95	0.452	0.441	0.669	0.567
1.0+7	4.717-9	5.104-9	9.820-9	12.96	0.455	0.034	0.012	0.023
5.0+7	6.255-10	9.803-11	7.235-10	12.97	0.452	0.201	0.011	0.175
1.0+8	1.995-10	3.427-11	2.338-10	12.96	0.440	0.569	0.029	0.490
5.0+8	4.145-11	1.951-11	6.095-11	12.89	0.378	1.208	0.023	0.829
1.0+9	2.785-11	1.352-11	4.137-11	12.86	0.347	0.646	0.012	0.439
5.0+9	1.257-12	7.301-13	1.987-12	12.84	0.329	0.004	0.0001	0.003
1.0+10	2.836-14	1.926-14	4.762-14	12.84	0.329	0.002	0.0019	0.002
5.0+10	2.086-16	2.296-16	4.383-16	12.85	0.329	0.272	0.159	0.213
1.0+11	2.068-16	2.276-16	4.345-16	12.85	0.329	0.275	0.160	0.215
5.0+11	1.941-16	2.125-16	4.066-16	12.85	0.329	0.293	0.171	0.229
1.0+12	1.796-16	1.953-16	3.750-16	12.85	0.329	0.316	0.186	0.248
5.0+12	1.068-16	1.073-16	2.141-16	12.87	0.327	0.528	0.337	0.433
1.0+13	7.084-17	6.262-17	1.335-16	12.87	0.325	0.791	0.574	0.689

*CALCULATIONS USE ENDF/B-IV DATA WITH CORRECTIONS LISTED IN LA-6116-MS. ACTUAL BURST DURATION = 1.0-4S.

TABLE XVIII

U235 THERMAL FISSION
INFINITE IRRADIATION*
2/20/76

COOLING TIME(S)	MEV/FISS BETA	MEV/FISS GAMMA	MEV/FISS TOTAL	% IN GAS PRODUCTS DENSITY TOTAL	DENSITY RADIO-ACTIVE	MEV/FISS BETA	MEV/FISS GAMMA	MEV/FISS TOTAL
0.0+0	6.4816+0	6.1284+0	1.2610+1	12.86	0.3269	19.72	24.46	22.03
2.0+0	5.6114+0	5.4854+0	1.1097+1	12.86	0.3269	20.05	25.08	22.54
5.0+0	5.0716+0	5.1007+0	1.0172+1	12.86	0.3269	19.94	25.20	22.58
1.0+1	4.5778+0	4.7489+0	9.3267+0	12.86	0.3269	19.77	25.29	22.58
2.0+1	4.0459+0	4.3435+0	8.3894+0	12.86	0.3269	19.34	25.32	22.44
5.0+1	3.3622+0	3.7458+0	7.1080+0	12.86	0.3269	18.06	25.18	21.81
1.0+2	2.8825+0	3.2819+0	6.1644+0	12.86	0.3269	16.75	25.16	21.23
2.0+2	2.4630+0	2.8602+0	5.3232+0	12.86	0.3269	15.42	25.57	20.87
5.0+2	2.0042+0	2.4045+0	4.4087+0	12.86	0.3269	14.15	26.99	21.15
1.0+0	1.6960+0	2.0873+0	3.7833+0	12.86	0.3269	13.97	28.82	22.16
2.0+3	1.4055+0	1.7484+0	3.1539+0	12.86	0.3269	14.71	31.49	24.01
5.0+3	1.0872+0	1.2969+0	2.3841+0	12.86	0.3269	15.29	34.71	25.85
1.0+4	9.0470-1	1.0112+0	1.9159+0	12.86	0.3269	14.34	33.90	24.66
2.0+4	7.4499-1	8.0248-1	1.5475+0	12.86	0.3269	13.28	30.75	22.34
5.0+4	5.5630-1	6.2336-1	1.1797+0	12.86	0.3269	12.74	26.94	20.24
1.0+5	4.4999-1	5.1934-1	9.6934-1	12.86	0.3269	10.91	23.34	17.57
2.0+5	3.8094-1	4.3422-1	8.1515-1	12.86	0.3269	8.095	19.19	14.00
5.0+5	3.2308-1	3.3888-1	6.6195-1	12.86	0.3269	4.693	11.76	8.310
1.0+6	2.8468-1	2.6612-1	5.5079-1	12.86	0.3269	2.349	5.358	3.803
2.0+6	2.4529-1	1.9710-1	4.4239-1	12.86	0.3269	0.8334	1.339	1.059
5.0+6	1.9457-1	1.2417-1	3.1874-1	12.86	0.3269	3.707-1	7.563-2	2.558-1
1.0+7	1.6040-1	8.5203-2	2.4560-1	12.86	0.3269	4.195-1	1.196-2	2.781-1
2.0+7	1.2992-1	5.4709-2	1.8462-1	12.86	0.3269	5.077-1	1.724-2	3.623-1
5.0+7	9.7309-2	3.9787-2	1.3710-1	12.86	0.3269	6.374-1	2.284-2	4.590-1
1.0+8	7.9180-2	3.7297-2	1.1648-1	12.86	0.3269	7.078-1	2.294-2	4.885-1
2.0+8	6.8679-2	3.4475-2	1.0315-1	12.86	0.3269	6.665-1	2.217-2	4.511-1

*CALCULATIONS USE ENDF/B-IV DATA WITH CORRECTIONS LISTED IN LA-6116-MS. INFINITE REFERS TO A CONSTANT FISSION RATE (NO DEPLETION) FOR 1.0+13S.

$h(t_c)$ = the energy release rate following a fission burst (units are normally MeV/fission/s),

and

$H(t_c,t_s)$ = energy release rate following a constant fission rate (units of Mev/fission) for time t_s and a cooling time t_c,

then

$$H(t_c,t_s) = \int_{t_c}^{t_c+} h(t)dt = \int_{t_c}^{\infty} h(t)dt - \int_{t_c+}^{\infty} h(t)dt$$

$$= H(t_c,\infty) - H(t_c + t_s,\infty) \quad .$$

Thus, either the burst function $h(t_c)$ or the decay heat function following a constant fission rate for an infinite time $H(t_c,\infty_s)$ can be used to give the results for a finite irradiation. The burst function is being fitted to a sum of exponentials for such use. Both types of functions will be used in revising the ANS 5.1 decay heat standard. However, there are small but necessary corrections for neutron absorption effects. These are also being evaluated.

The gas content is similar to results reported earlier for fast fission,[70] but we now have detailed tables for each gas. (In ENDF/B-IV, there are 93 gases, ~80 being radioactive.) The results are particularly pertinent for several benchmark short-cooling-term decay-heating experiments currently in progress where one must consider the possibility of gas loss. For example, one experiment has used an irradiation period of 24 h followed by measurements of beta and gamma heating out to 10^5 s. For this case, and at a cooling time of 10^4 s, the radioactive gas products account for only 8% of the total number of fission products, but these contribute 45% of the gamma energy release rate. Figures 17 and 18 show the temporal variations of all gases and noble gases.

Aggregate beta and gamma spectra from the gaseous products and from the total fission product ensemble are now being computed and compared with various experiments at LASL and other laboratories. Comparisons with recent preliminary LASL experiments of gamma spectra are extremely encouraging; the

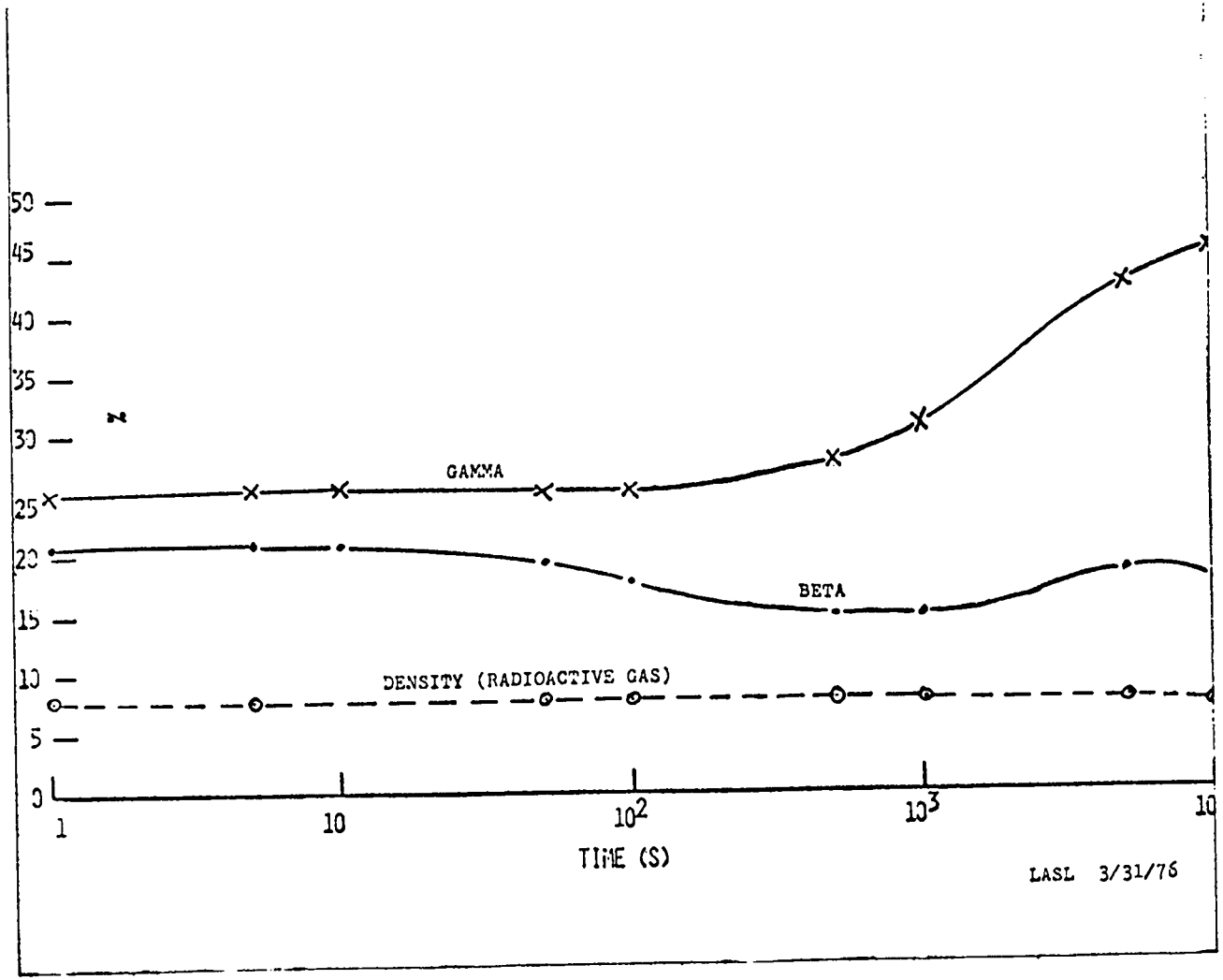

Fig. 17. % MeV/Fiss and density in noble gas and halogens of all fission products. (^{235}U thermal fission for 24 hours).

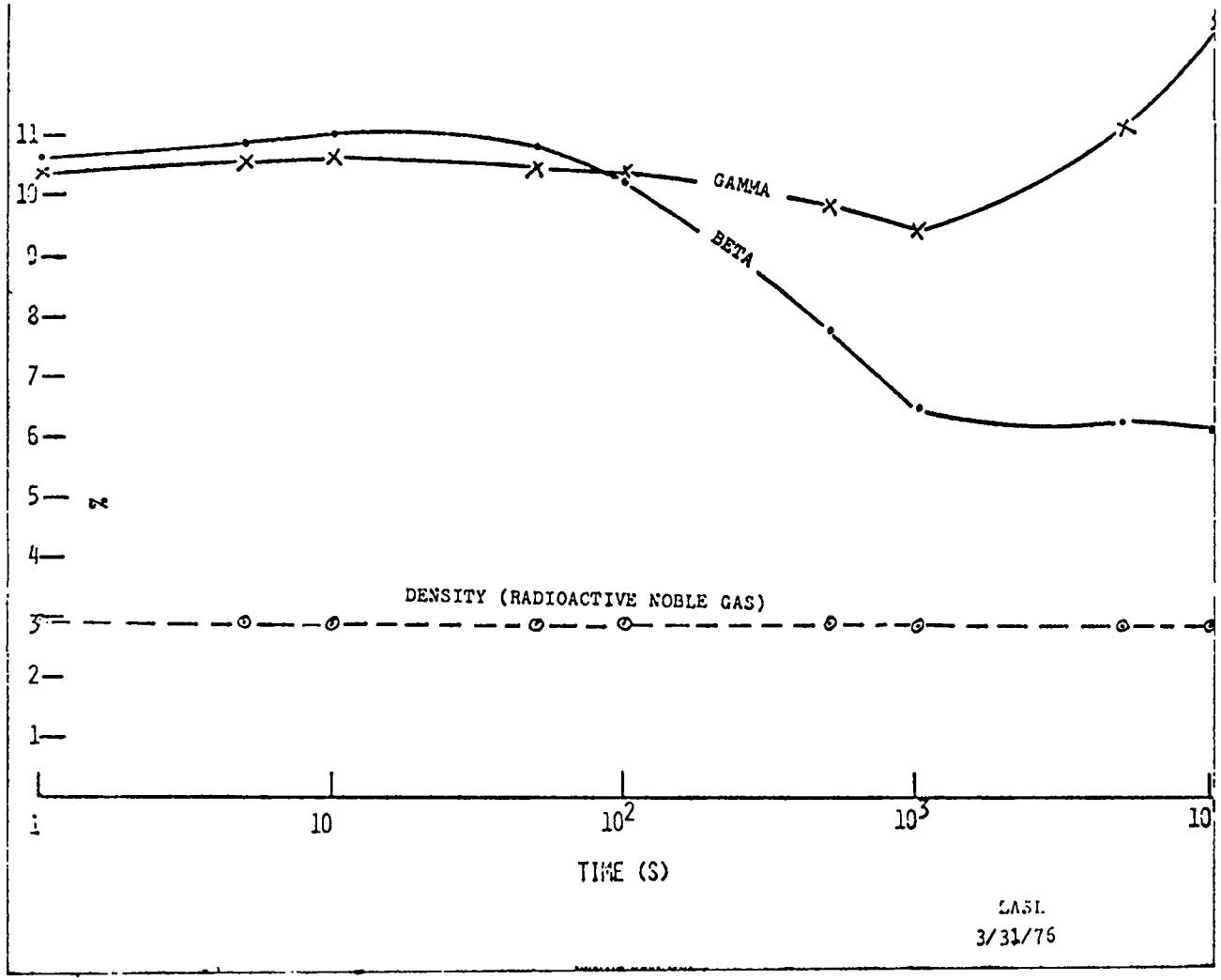

Fig. 18. % MeV/Fiss and density in noble gases of all fission products. (^{235}U thermal fission for 24 hours).

total gamma release rates from 152 s to 42 h agree with the pilot experiments within 6% or better at all cooling times. Spectral and decay heat comparisons will be presented at the Toronto American Nuclear Society meeting[71] in June, 1976. Comparisons of total gamma heating calculations with preliminary ORNL measurements were presented in the previous progress report.[72]

Sample calculations of beta and gamma spectra are shown in Figs. 19 and 20. These apply to the case of constant ^{235}U thermal fission for 24 h and at a cooling time of 1000 s. Fifteen beta groups (500-keV wide) and 150 gamma groups (50-keV wide) were used. The gamma lines in this sample are energy broadened for comparison with experiments. Spectral and decay heating data are being supplied to the Intelcom Rad Tech Corporation for assistance in analysis of their experiments currently in progress.

Version-7 of the CINDER code was supplied to Sandia, GE, and the Air Force Tactical Air Command during this quarter, and assistance was given to Sandia and GE in getting the code operational.

VI. MEDIUM ENERGY LIBRARY (D. G. Foster, Jr. and H. M. Holleman)

All of the existing medium-energy history tapes have been transferred to photostore except those for a ^{238}U target. The ^{238}U data sets are of questionable use, however, inasmuch as CROIX has no fission channel in its evaporation module.

Processing of histories for ^{12}C, ^{16}O, ^{27}Al, and ^{56}Fe into the National Aeronautics and Space Administration equiprobability-boundary format has been completed. A complete tape of the output and microfiche copes of the printouts will be shipped in April.

Some additional work has been done on the program which converts the equiprobability boundaries into differential cross sections. Efforts to obtain stable fits in the neighborhood of the kinematic cutoff at high secondary-particle energies by constraining the fits to go to zero along a line or at selected points have been fairly successful. To date, however, no single algorithm has been devised which never gives negative cross sections within the kinematically-accessible region of angle and energy.

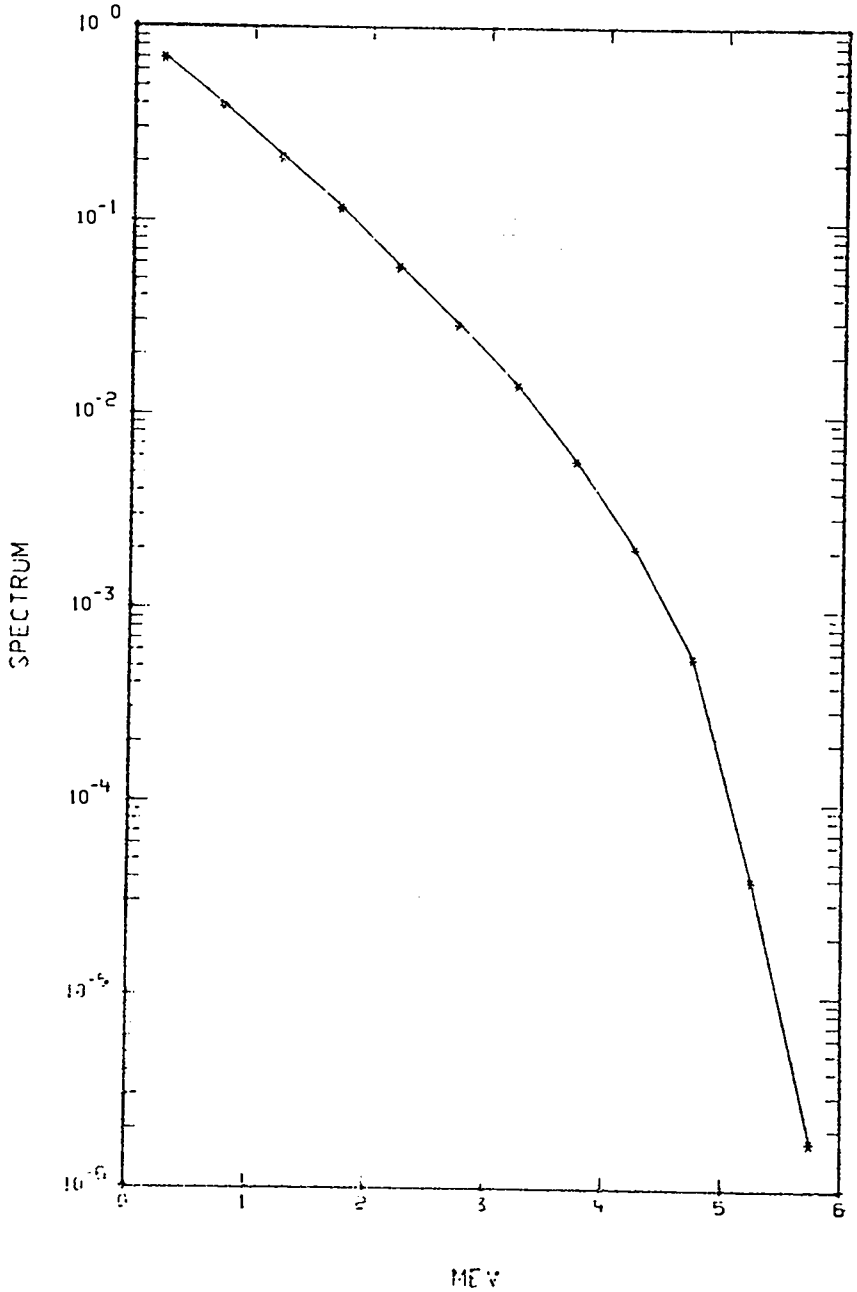

Fig. 19. Betas/fission after 24 hours ^{235}U thermal irradiation and 1000 seconds cooling.

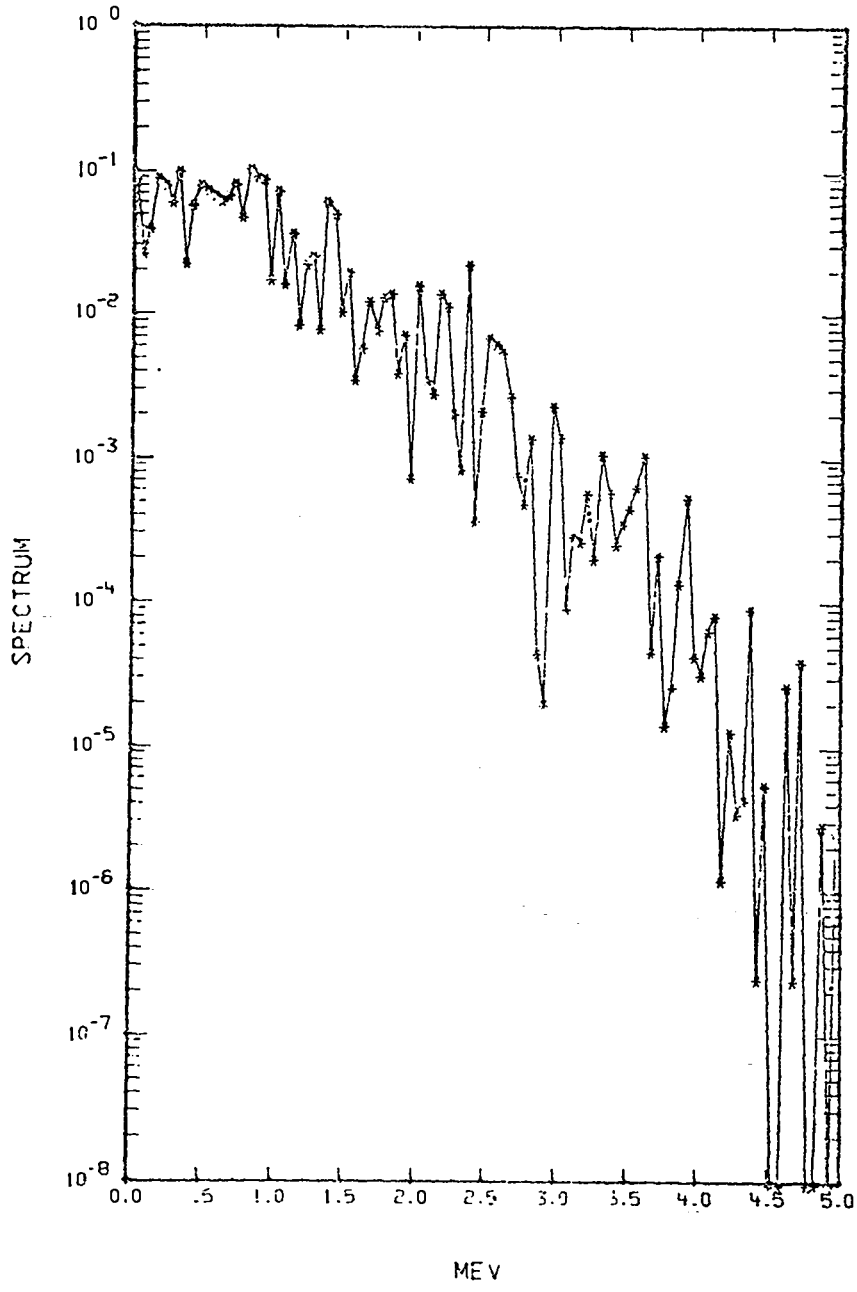

Fig. 20. Gamma/fission after 24 hours ^{235}U thermal irradiation and 1000 seconds cooling.

REFERENCES

1. G. M. Hale, "R-Matrix Analysis of the Light Elements Standards," Nuclear Cross Sections & Technology Conference Proceedings ,NBS Special Publication 425, Vol. 1, p. 302 (1975).

2. N. Jarmie, G. G. Ohlsen, P. A. Lovoi, R. J. Barrett, G. M. Hale, and D. C. Dodder, "Elastic Scattering of 7-12 MeV Tritons by Alpha Particles," Bull. Am. Phys. Soc. 20, 596 (1975).

3. R. A. Hardekopf, N. Jarmie, G. G. Ohlsen, and F. V. Moore, "Analyzing Power for $^{4}He(t,t)^{4}He$ Elastic Scattering," Proc. Fourth International Symposium on Phenomena in Nuclear Reactions, Zurich, 1975 (to be published).

4. J. A. Harvey and N. W. Hill, "Neutron Total Cross Section of ^{6}Li from 10 eV to 10 MeV," Nuclear Cross Sections and Technology Conference Proceedings, NBS Special Publication 425, Vol. 1, p 244 (1975).

5. G. Lamaze, National Bureau of Standards, private communication (1976).

6. R. Schrack, National Bureau of Standards, private communication (1976).

7. R. M. Sealock and J. C. Overley, "$^{10}B(n,\alpha)^{7}Li^{*}$ Differential Cross Section Measurements between 0.2 and 1.25 MeV," submitted to Phys. Rev. C (1976); R. M. Sealock, "A Measurement of Differential Cross Sections for the $^{10}B(n,\alpha)^{7}Li,^{7}Li*$ Reactions," Dissertation, University of Oregon, unpublished (1975).

8. E. D. Pendlebury, "Neutron Cross Sections of Li-6 in the Energy Range 0.001 eV - 15 MeV," Atomic Weapons Research Establishment report AWRE 0-60/64 (July 1964) and "Neutron Cross Sections of Li-7 in the Energy Range 0.001 eV - 15 MeV," Atomic Weapons Research Establishment report AWRE 0-61/64.

9. D. W. Muir and P. G. Young, "Applied Nuclear Data Research and Development, April 1-June 30, 1975," Los Alamos Scientific Laboratory report LA-6123-PR, p. 2 (1975).

10. John C. Hopkins, D. M. Drake, and H. Conde, "Elastic and Inelastic Scattering of Fast Neutrons from ^{6}Li and ^{7}Li," Nuclear Phys. A107, 139 (1968) and Los Alamos Laboratory report LA-3765 (1967).

11. G. M. Frye, Jr., L. Rosen, and L. Stewart, "Disintegration of Carbon into Three Alpha Particles by 12-20 MeV Neutrons," Phys. Rev. 99, 1375 (1955).

12. B. Antolkovic and Z. Dolenec, "The Neutron-Induced $^{12}C(n,n')3\alpha$ Reaction at 14.4 MeV in a Kinematically Complete Experiment," Nucl. Phys. A237, 235 (1975).

13. F. Ajzenberg-Selove and C. L. Busch, University of Pennsylvania, "Nuclear Wallet Cards," distributed by American Institute of Physics (Dec. 1971).

14. L. R. Veeser and E. D. Arthur, "Measurement of (n,2n) and (n,3n) Cross Sections," Bull. Am. Phys. Soc. 20, 1196 (1975).

15. B. P. Bayhurst, J. S. Gilmore, R. J. Prestwood, J. B. Wilhelmy, Nelson Jarmie, B. H. Erkkila, and R. A. Hardekopf, "Cross Sections for (n,xn) Reactions between 7.5 and 28 MeV," Am. Phys. Soc. 20, 1196 (1975).

16. L. Milazzo-Colli and G. M. Braga-Marcazzan, "α - Emission by Pre-equilibrium Processes in (n,α) Reactions," Nucl. Phys. A210, 297 (1973).

17. R. C. Haight, S. M. Grimes, B. J. Tuckey, and J. D. Anderson, "A Charged Particle Spectrometer for Neutron Induced Reactions," Lawrence Livermore Laboratory preprint UCRL-7151 (1975).

18. B. J. Allen, R. J. Macklin, R. R. Winters, and C. Y. Fu, "Neutron-Capture Cross Sections of the Stable Lead Isotopes," Phys. Rev. C8, 1504 (1973).

19. D. Wilmore and P. C. Hodgson, "The Calculation of Neutron Cross Sections from Optical Potentials," Nucl. Phys. 55, 676 (1964).

20. D. M. Brink, Oxford University, thesis (1955); P. Axel, "Electric Dipole Ground State Transition Width Strength Function," Phys. Rev. 126, 671 (1962).

21. K. J. Schneider and A. M. Platt, Eds., "Advanced Waste-Management Studies, High-Level Waste Disposal Alternatives," Battelle Pacific Northwest Laboratory report BNWL-1900 (Vol. 4), Appendix C of Sec. 9, p. 9.C.19 (1974).

22. R. B. Kidman and R. E. MacFarlane, "LIB-IV, A Library of Group Constants for Nuclear Reactor Calculations," Los Alamos Scientific Laboratory report LA-6260-MS (March 1976).

23. R. B. Kidman and R. E. MacFarlane, "CINX: Collapsed Interpretation of Nuclear X Sections," Los Alamos Scientific Laboratory report LA-6287-MS (1976).

24. R. E. MacFarlane and R. B. Kidman, "LINX and BINX: CCCC Utility Codes for the MINX Multigroup Processing Code," Los Alamos Scientific Laboratory report LA-6219-MS (February 1976).

25. E. A. Straker, "Suggested Energy Group Bounds for a General Purpose Photon Multigroup Cross Section Set," Science Applications, Inc. report SAI-74-566-HV (July 1974).

26. K. D. Lathrop, "GAMLEG - A FORTRAN Code to Produce Multigroup Cross Sections for Photon Transport Calculations," Los Alamos Scientific Laboratory report LA-3267 (April 1965).

27. J. H. Hubbell, W. J. Veigile, E. A. Briggs, R. T. Brown, D. T. Cromer, and R. J. Howerton, "Atomic Form Factors, Incoherent Scattering Functions, and Photon Scattering Cross Sections," J. Phys. Chem. Ref. Data 4, 471 (1975).

28. B. M. Carmichael, "Standard Interface Files and Procedures for Reactor Physics Codes, Version III," Los Alamos Scientific Laboratory report LA-5486-MS (1974).

29. Y. D. Naliboff and J. U. Koppel, "HEXSCAT, Coherent Elastic Scattering of Neutrons by Hexagonal Lattices," General Atomic report GA-6026 (1974).

30. M. M. R. Williams, The Slowing Down and Thermalization of Neutrons (John Wiley and Sons, New York, 1966) p. 38.

31. R. J. LaBauve, C. R. Weisbin, R. E. Seamon, M. E. Battat, D. R. Harris, P. G. Young, and M. M. Klein, "PENDF: A Library of Nuclear Data for Monte Carlo Calculations Derived from Data in ENDF/B Format," Los Alamos Scientific Laboratory report LA-5687 (1974).

32. E. D. Cashwell, J. R. Neergaard, W. M. Taylor, and G. D. Turner, "MCN: A Neutron Monte Carlo Code," Los Alamos Scientific Laboratory report LA-4751 (1972).

33. D. E. Cullen, O. Ozer, and C. R. Weisbin, "Tabular Cross Section File Generation and Utilization Techniques," Nuclear Cross Sections & Technology Conference Proceedings, NBS Special Publication 425, Vol. 1, p 419 (1975).

34. L. B. Levitt, "The.Probability Table Method for Treating Unresolved Neutron Resonances in Monte Carlo Calculations," Nucl. Sci. Eng. 49, 450 (1972).

35. S. Pearlstein, "Resonance Region Analysis Without Resonance Parameters," Nucl. Sci. Eng. 58, 354 (1975).

36. R. E. MacFarlane and R. M. Boicourt, "NJOY: A Neutron and Photon Cross-Section Processing System," Trans. Am. Nucl. Soc. 22, 720 (1975).

37. I. Bondarenko, Ed. Group Constants for Nuclear Reactor Calculations (Consultants Bureau, New York, 1964).

38. R. B. Kidman, R. E. Schenter, R. E. Hardie, and W. W. Little, "The Shielding Factor Method of Generating Multigroup Cross Sections for Fast Reactor Analysis," Nucl. Sci. and Eng. 48, 198 (1973).

39. R. W. Hardie and W. W. Little, Jr., "1DX, A One-Dimensional Diffusion Code for Generating Effective Nuclear Cross Sections," Battelle Northwest Laboratory report BNWL-954 (1969).

40. R. E. MacFarlane and Martin Becker, "Self-Shielded Cross Sections for Neutron Transport in Iron," Trans. Am. Nucl. Soc. 22, 668 (1975).

41. R. B. Kidman and R. E. Schenter, "Group Constants for Fast Reactor Calculations," Hanford Engineering Development Laboratory report HEDL-TME-71-36 (1971).

42. B. K. Malaviya, N. N. Kaushal, M. Becker, E. T. Burns, A. Ginsberg, and E. R. Gaerttner, "Experimental and Analytical Studies of Fast Neutron Transport in Iron," Nucl. Sci. Eng. 47, 329 (1972).

43. N. C. Paik and W. Davis, SPHINX Development covered in Westinghouse Advanced Reactors Division Quarterly Progress reports WARD-XS-3045-4 through 7 (1973-1974).

44. N. G. Demas, Westinghouse Nuclear Energy Systems, private communication.

45. B. J. Toppel, A. L. Rago, and D. M. O'Shea, "MC^2, A Code to Calculate Multigroup Cross Sections," Argonne National Laboratory report ANL-7318 (1967).

46. R. Roussin, Radiation Shielding Information Center, Oak Ridge National Laboratory, private communication.

47. M. M. Levine, "Resonance Integral Calculations for ^{238}U Lattices," Nucl. Sci. Eng. 16, 271 (1963).

48. M. G. Stamatelatos, "Cross Section Space Shielding in Doubly Heterogeneous HTGR Systems," Los Alamos Scientific Laboratory report LA-6157-MS (1975).

49. A. Sauer, "Approximate Escape Probabilities," Nucl. Sci. Eng. 16, 329 (1963).

50. D. W. Muir and P. G. Young, "Applied Nuclear Data Research and Development, April 1 - June 30, 1975," Los Alamos Scientific Laboratory report LA-6123-PR (1975), Sec. VI-A, p. 12.

51. D. W. Muir and P. G. Young, "Applied Nuclear Data Research and Development, April 1 - June 30, 1975," Los Alamos Scientific Laboratory report LA-6123-PR (1975), Sec. VI-B, p. 12.

52. D. R. Harris, W. A. Reupke, and W. B. Wilson, "Consistency Among Differential Nuclear Data and Integral Observations: The ALVIN Code for Data Adjustment, for Sensitivity Calculations, and for Identification of Inconsistent Data," Los Alamos Scientific Laboratory report LA-5987 (1975).

53. W. A. Reupke and D. W. Muir, "Consistency Analysis of Fusion Reactor Neutronics Data: Tritium Production," Trans. Am. Nucl. Soc. Toronto Meeting (June 1976).

54. D. W. Muir and M. E. Wyman, "Neutronic Analysis of a Tritium Production Integral Experiment," Proc. of Tech. of Controlled Thermonuclear Fusion Experiments and the Engineering Aspects of Fusion Reactors Conf., CONF-721111 (1972) p. 910.

55. M. E. Wyman, "An Integral Experiment to Measure the Tritium Production from ^{7}Li by 14-MeV Neutrons in a Lithium Deuteride Sphere," Los Alamos Scientific Laboratory report LA-2234-Rev (November 1972).

56. D. R. Harris, P. G. Young, and G. M. Hale, "Characterization of Uncertainties in Evaluated Cross-Section Sets," Trans. Am. Nucl. Soc. 16, 323 (1973).

57. D. W. Muir and P. G. Young, "Applied Nuclear Data Research and Development, April 1 - June 30, 1975," Los Alamos Scientific Laboratory report LA-6123-PR, (1975) Sec. V-A, p. 11.

58. A. C. Wahl, "Nuclear Charge Distribution in Fission: Cumulative Yields of Short-Lived Krypton and Xenon Isotopes from Thermal-Neutron Induced Fission of ^{235}U," J. Inorg. Nucl. Chem. 6, 263 (1958).

59. M. E. Meek and B. F. Rider, "Compilation of Fission Product Yields," General Electric publication NEDO-12154-1 (1974).

60. K. Wolfsberg, "Estimated Values of Fractional Yields from Low Energy Fission and A Compilation of Measured Fractional Yields," Los Alamos Scientific Laboratory report LA-5553-MS (1974).

61. J. O. Rasmussen, W. Norenberg, and H. J. Mang, " A Model for Calculating the Angular Momentum Distribution of Fission Fragments," Nucl. Phys. A136, 465 (1969).

62. K. Dietrich, "Summary of the Symposium," Proc. of Internl. Atomic Energy Agency on Physics and Chemistry of Fission, Vol. II, 461 (1973).

63. R. D. Evans, The Atomic Nucleus (McGraw Hill Book Co., New York, 1955), p. 552.

64. E. J. Konopinski, The Theory of Beta Radioactivity (Oxford University Press, Oxford, England, 1966) p. 14.

65. T. R. England, "An Investigation of Fission Product Behavior and Decay Heating in Nuclear Reactors," Thesis, University of Wisconsin (1969).

66. T. R. England and R. E. Schenter, "ENDF/B-IV Fission Product Files: Summary of Major Nuclide Data," Los Alamos Scientific Laboratory report LA-6116-MS (ENDF 223) (September 1975).

67. R. J. LaBauve and W. B. Wilson, "Proposal to Extend CSEWG Neutron and Photon Multigroup Structures for Wider Applications," Los Alamos Scientific Laboratory report LA-6240-P (Feb. 1976).

68. C. R. Weisbin, P. D. Soran, R. E. MacFarlane, D. R. Harris, R. J. White, J. S. Hendricks, J. E. White, and R. B. Kidman, "MINX: A Multigroup Interpretation of Nuclear X Sections from ENDF/B," Los Alamos Scientific Laboratory report (to be published).

69. T. R. England, R. Wilczynski, and N. L. Whittemore, "CINDER-7: An Interim Report for Users," Los Alamos Scientific report LA-5885-MS (April 1975).

70. T. R. England, R. E. Schenter, and N. L. Whittemore, "Gamma and Beta Decay Power Following ^{235}U and ^{239}Pu Fission Bursts," Los Alamos Scientific Laboratory report LA-6021-MS (July 1975).

71. T. R. England and M. G. Stamatelatos, "Beta and Gamma Spectra and Total Decay Energies from Fission Products," Trans. Am. Nucl. Soc., June 1976 Toronto Meeting.

72. C. I. Baxman and P. G. Young, "Applied Nuclear Data Research and Development, October 1 - December 31, 1975," Los Alamos Scientific Laboratory report LA-6266-PR (March 1976).

☆ US GOVERNMENT PRINTING OFFICE: 1976—677-343/190